

## **Sensitivity of interval Vp/Vs analysis of seismic data**

Rafael Asuaje, Don C. Lawton

### **SUMMARY**

The ratio of a compressional P wave to a shear S wave is of great importance for converted PS wave applications. Dipole sonic logs can provide accurate velocity ratio calculations but are restricted to the location of the corresponding well. Isochrons from interpreted horizons on seismic data can provide information on Vp/Vs throughout the volume that can be used for lithology and fluids studies about a particular formation. Proper interpretations of these events are necessary to avoid erroneous results. The objective of this paper is to set guidelines for an interpreter to accurately pick events and understand the error that can be expected from various isochron intervals to ultimately suggest a minimum interval time that can provide accurate Vp/Vs values.

In a study on the Hussar data set, based on the increasing observable error with respect to decrease in the time intervals, as well as taking into consideration the variability of the Vp/Vs values due to uncertainty it is suggested to use isochron intervals greater than 150ms. Interval Vp/Vs analysis for data with intervals greater than this time presented low uncertainty.

### **INTRODUCTION**

Compressional P waves have dominated the oil industry for the past 60 years because they have generally provided better resolution than shear S waves. P waves can travel through fluids and the particle motion is parallel to the direction of propagation. On the other hand, shear S waves travel at approximately half the speed of the compressional wave and are transverse waves. S waves do not propagate through liquids due to shear modulus being zero in this medium, so they are not available in a marine environment. Through the analysis of multicomponent seismic data, important rock properties such as Vp/Vs can be extracted. This paper uses the interpretation of both PP waves and PS waves to help calculate Vp/Vs ratios throughout the entire seismic section. In addition, synthetic models are used to compare results from ideal conditions to those from the real data analysis.

The ratios of compressional and shear waves are key to the determination of lithology as well as to the identification of pore fluids using, for example, AVO analysis. The Hussar data already has dipole sonic logs in one of the wells and, through a Castagna relationship, shear logs were modelled for the remaining wells. The principle objective of this document is to set guidelines for horizon interpretation and suggest a minimum interval time for robust Vp/Vs analysis.

## Hussar Data

The Hussar experiment was performed in 2011 in association with CREWES and the sponsors INOVA, Geokinetics, and Husky Energy (Margrave et al. 2011). The location for this particular experiment was near Hussar, Alberta, about 100km east from the city of Calgary. This site was chosen because of its close proximity to the University of Calgary and to various wells. The three closest wells to the seismic line were studied. Well 12-27 had a dipole sonic tool that recorded P-wave and S-wave sonic velocities. In addition, it had density and gamma-ray logs. Both wells 14-27 and 14-35 had a monopole sonic tool that only allowed P-waves to be recorded. Density and gamma-ray logs were also available in these wells.

The seismic line extended for 4.5km from northeast to southwest and consisted of 10Hz 3C geophones (Figure 1). Four hundred forty-eight geophones were laid out on this line in intervals of 10m. Dynamite was a source for the seismic data recorded on this line.



FIG. 1: Location of the Hussar seismic line with nearby wells, and shot locations. Well 12-27 provided dipole sonic logs; wells 14-27 and 14-35 only provided P-wave logs. (Margrave et al., 2011).

The seismic section was processed in order to attenuate the surface waves and undesirable wavetrains while attending to keep the broadband frequency content of the reflection data. Isaac and Margrave (2011) analysed and processed the dataset, with radial trace filter and gabor deconvolution applied for noise attenuation. Static corrections were also applied and the data was post-stack Kirchhoff time migrated. As little processing as possible was done so that the frequency content of the signal would not be compromised (Isaac and Margrave, 2011). FX filtering and band-pass filters were applied to each seismic section (Figures 2 and 3) to improve the signal.

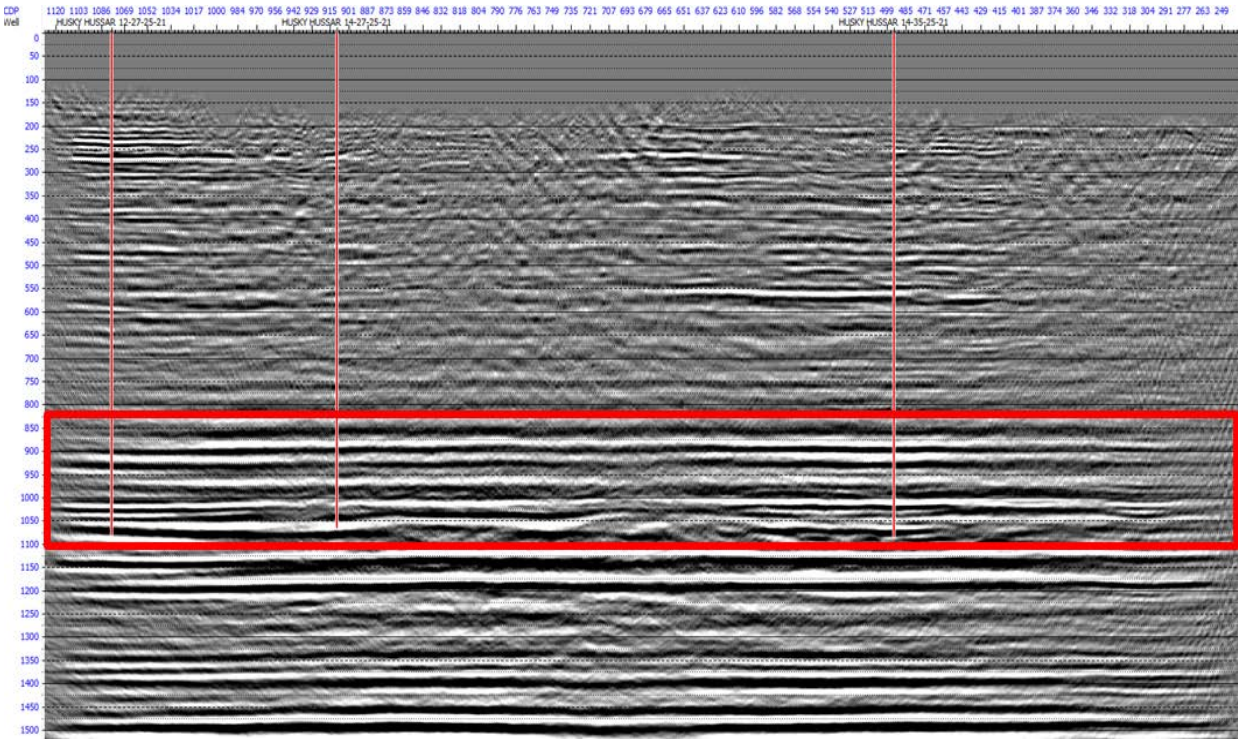


FIG. 2: Hussar PP volume seismic section; the red rectangle indicates the area of investigation; well locations are indicated by the vertical red lines.

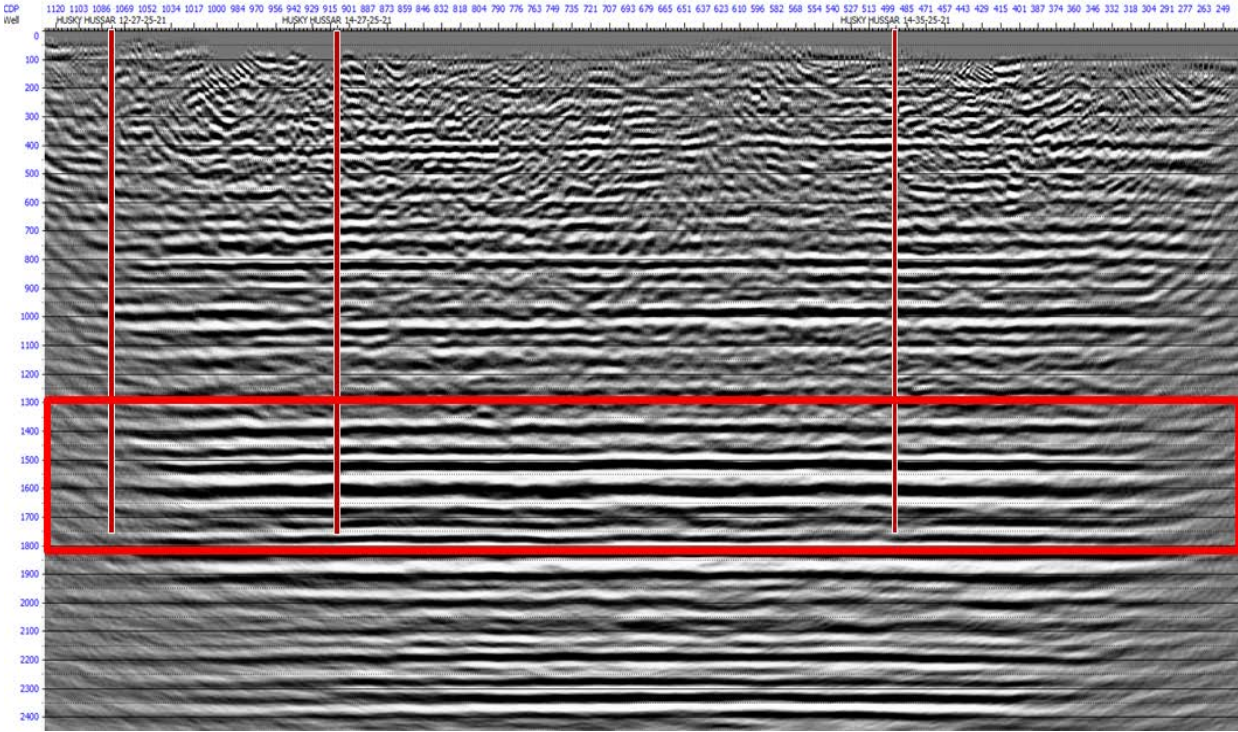


FIG. 3: Hussar PS volume seismic section; the red rectangle indicates the area of investigation; the uncorrelated well locations are indicated by the vertical red lines.

## Geological Overview

The data location is in Central Alberta and is characterized by plains where the underlying surface formations are Cretaceous and Tertiary relative soft and flat beds (Allan and Rutherford, 1934).

The formation of interest for the horizon picks is the Manville Group, which belong to the oldest Cretaceous rock and represents a major episode of subsidence and sedimentation following a long period of uplift, exposure and erosion of older strata (Mossop and Shetsen, 1994). Mannville Group (Figure 4) is less than 40m thick in some parts, but in the Rocky Mountain foothills it is more than 700m thick. Gas and oil are trapped in fluvial reservoir sandstones in the south and in shoreline sandstone units throughout northern and central regions (Smith et al., 1994). The Manville Group is disconformably overlain by the Joli Fou Formation shale of the Colorado Group and it is underlain by older Paleozoic carbonates (Mossop and Shetsen, 1994).

This group also consists of inter-bedded continental sand and shale in the base (Detrital and Eilerslie Member), followed by calcareous sandstone member, marine shale (Ostracod beds) and Glauconitic Sandstones. The Glauconitic/Bluesky strata record the maximum transgression and subsequent early regressive stages of the lower Cretaceous Sea in the southern and central parts of the Basin. Marine evidence prevails in the Glauconitic Sandstone in Central Alberta and in the Bluesky Formation in northern Alberta (Gavotti and Lawton, 2014).

The Glauconitic Sandstone consists of very fine to medium quartz-rich sandstone in eastern Alberta and quartz sandstone intermixed with coarser sandstone in the western part of the province. Commonly, the Glauconite content decreases and clay content increases in southern Alberta, where the unit becomes less marine.

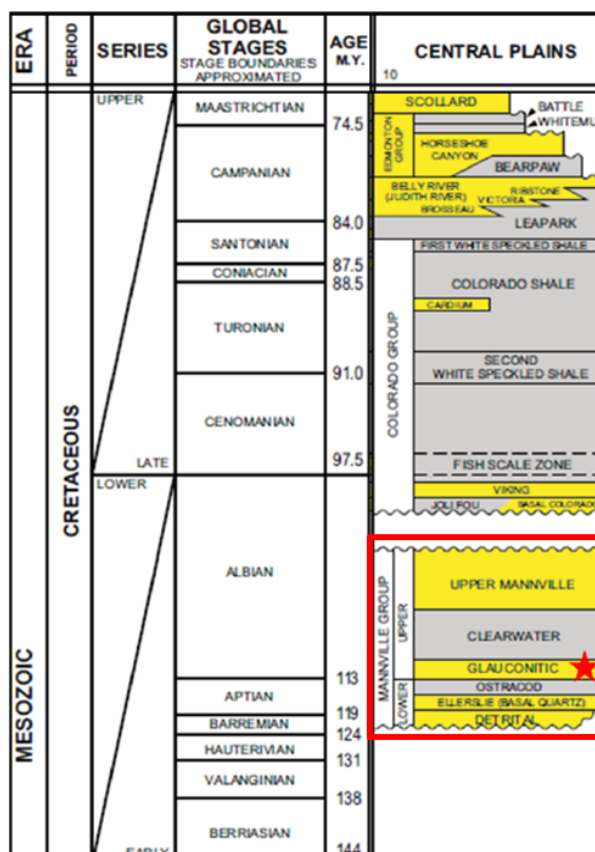


FIG. 4: Stratigraphic column for the Mannville group; the red star indicates the Glauconitic Formation (modified from Gavotti and Lawton, 2014).

## PS Converted wave seismic data

A converted wave is a wave that propagates downward as a P-wave and converts, on reflection, to an S-wave going upward (Figure 5). An advantage of using PS seismic data rather than only PP data is that converted waves can provide improved subsurface images as well as a measure of S-wave properties related to rock type and saturations. That is to say, PS will provide more information about the lithology of the area of study (Stewart et al., 2002). Other applications for PS data include internal Vp/Vs analysis.

Converted PS waves possess an asymmetrical ray-path which is described by Snell's law:  $\sin\theta/V_p = \sin\phi/V_s$ , where the angles  $\theta$  and  $\phi$  are the angles of incidence and reflection of P and S, respectively. Vp and Vs are the P and S velocities, respectively. Since P-waves travel faster than S-waves, Vp is greater than Vs. Also, the S-wave leaves the interface closer to the normal than the incident P-wave because  $\theta$  is greater than  $\phi$ .

Therefore, the reflection or conversion point is not midway between the source and the receivers. This conversion point is shifted forward towards the receiver for shallower reflections and larger Vp/Vs values (Stewart et al., 2002)

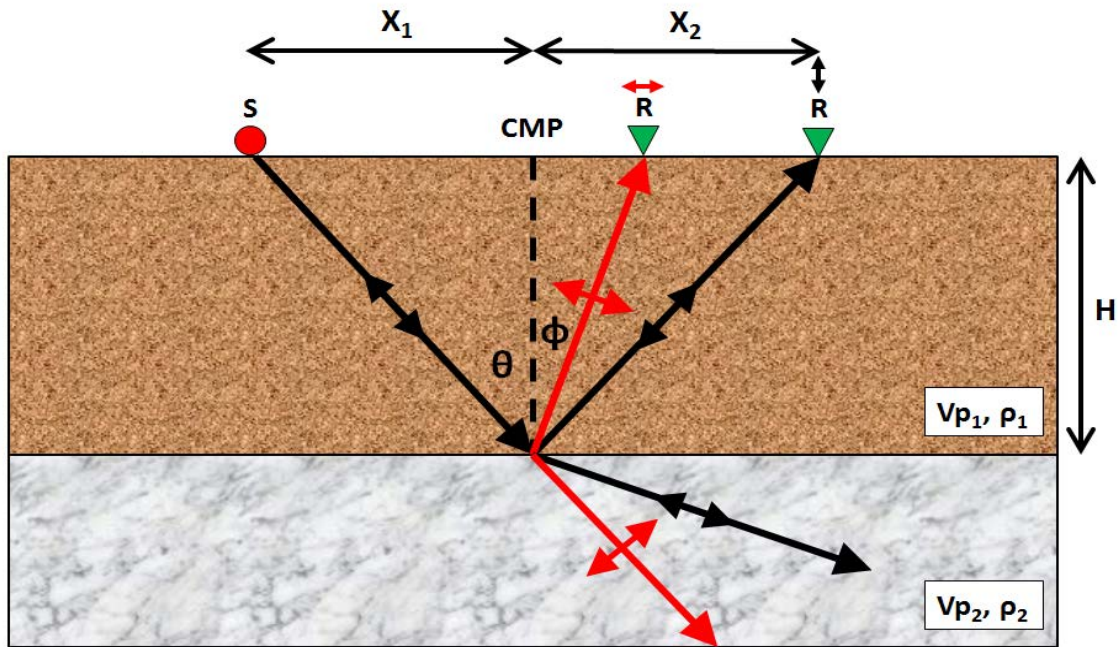


FIG. 5: PS converted wave and PP wave reflection and transmission through an interface. The common midpoint (CMP) is half the distance between the source and receiver on the PP wave.

### Wavelet and Resolution

On both PP and PS sections, the statistical wavelets were extracted at the well locations. Ormsby wavelets were defined by the frequencies 5-10-80-100 for PP and 10-15-80-100 for PS. In order to achieve zero phase a rotation was applied to the seismic data of both sections; the amount of rotation is determined by rotating the extracted wavelet until it is approximately symmetrical to the desired polarity. Figure 6 and 7 show the final multi-well wavelets extracted from the wells 14-27 and 14-35 with their amplitude spectra for both the PP and PS sections.

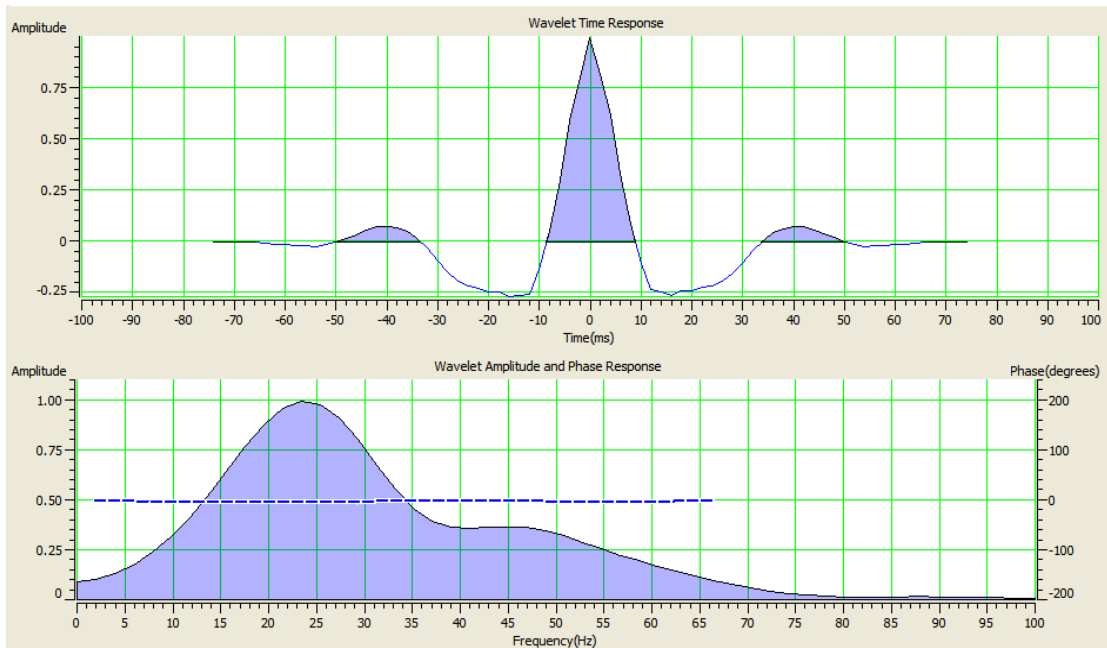


FIG. 6: PP section multi-well wavelet extracted from the wells 14-27 and 14-35 with its amplitude spectrum; the dotted blue line indicates the wavelet's average phase.

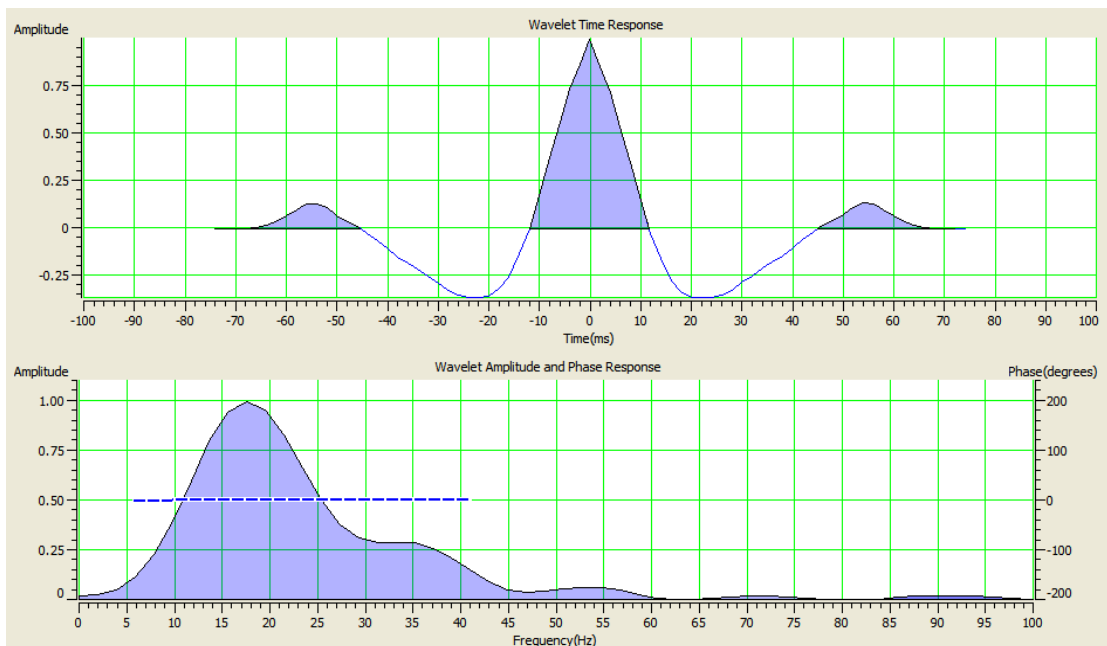


FIG. 7: PS section multi-well wavelet extracted from the wells 14-27 and 14-35 with its amplitude spectrum; the dotted blue line indicates the wavelet's average phase.

For practical purposes, the tuning thickness can be considered as an indicator of the vertical resolution. Widess (1973) claimed that bed thickness would be barely detectable if the bed had a thickness  $1/8$  of the wavelength. The Rayleigh criterion is the generally accepted criterion for vertical resolution; it defines the limit of resolution at  $1/4$  of the

dominant wavelength. From the seismic data, our period was approximately 25ms and our dominant frequency was 40Hz (Figure 8). The average compressional velocity at our point of investigation was 3400m/s and the vertical thickness at our point of interest was approximately 21m.

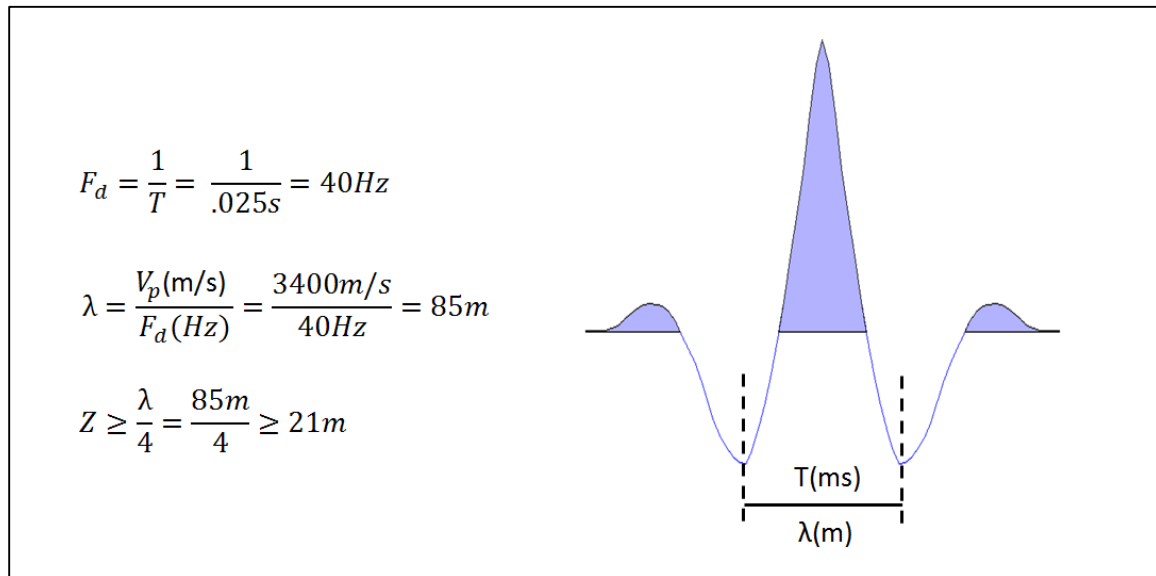


FIG. 8: The calculation for the minimum bed thickness that can be resolved;  $Z$  is the minimum thickness,  $F_d$  is the dominant frequency,  $T$  is the wavelength period, and  $\lambda$  represents the wavelength.

### Well Tie PP Procedure

Well ties are performed with the objective of relating stratigraphic markers in the wells to events on the seismic section; this helps with the horizon identification interpretation (Simm and Bacon, 2014). After extracting the statistical wavelet from the seismic data, the next step was to extract a wavelet from each well to refine the correlation. Ultimately, a final multi-wavelet was extracted from the wells 14-27 and 14-35 due to their similarities in their phases. This final multi-well wavelet, when convolved to the reflectivity from each well, helped with the creation of well synthetic seismograms at each well. Since check shots were not available, the next step was to apply a manual check shot correction by applying bulk shift to the synthetic to match a known strong event on the seismic. The bulk shift was required because the software used extrapolated the first  $V_p$  value to surface and it usually overestimates the near surface velocity (ProMC workshop, 2014). Finally, stretch or squeeze was performed to the logs to modify the time-depth curve to match the measured P-wave seismic times.

The wavelet extraction time window for each well in the PP section ranged from 600 ms to 1200 ms, which covered the depth interval of investigation. A bulk shift was applied to the synthetics in order to match the well tops to a known interpreted event in

the seismic section. Minor stretching was performed to fix mis-ties and to have a better correlation without modifying the sonic logs.

After horizons were picked on the PP and PS sections, the wells ties on the PS section were performed. The wavelet extraction time window for each well ranged from 900 ms to 1800 ms. Correlation in the PS section is lower in comparison to the PP section due to the lower resolution in the PS seismic section. Figure 9 to 11 show the results for the well ties on the PP section.

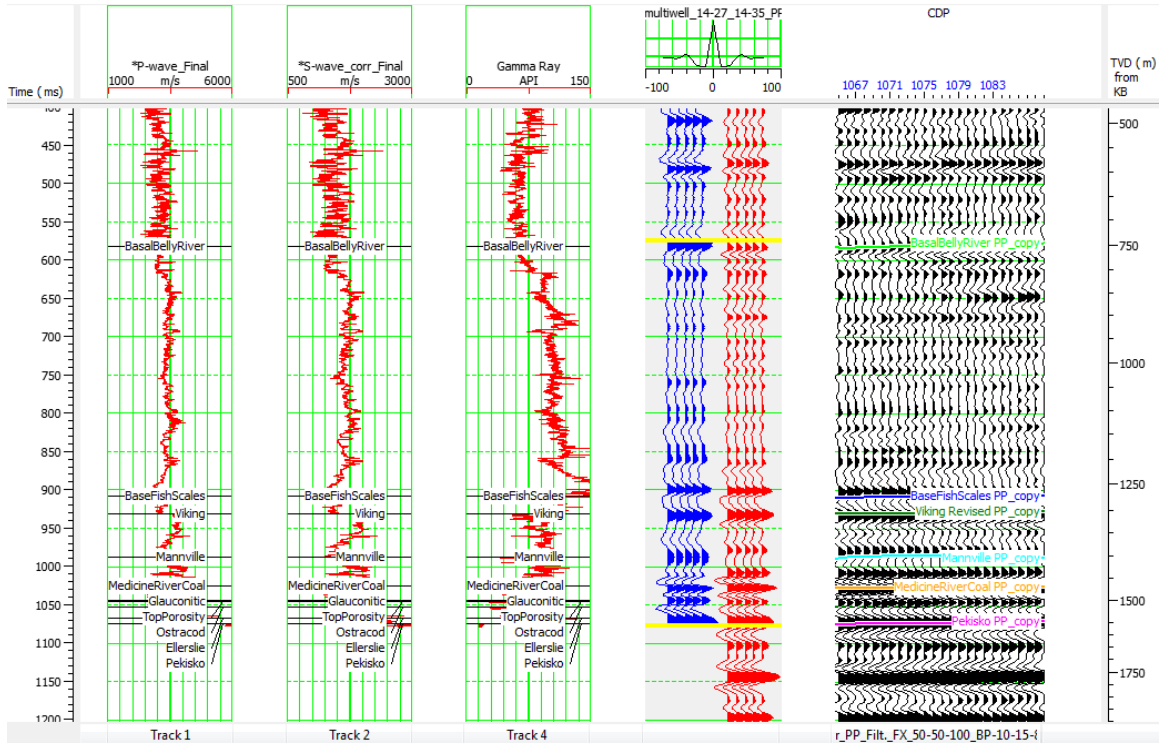


FIG. 9: The final tie of well 12-27 on the PP section; the blue traces represent the synthetic seismogram and the red traces are the extracted trace from the seismic data near the well location.

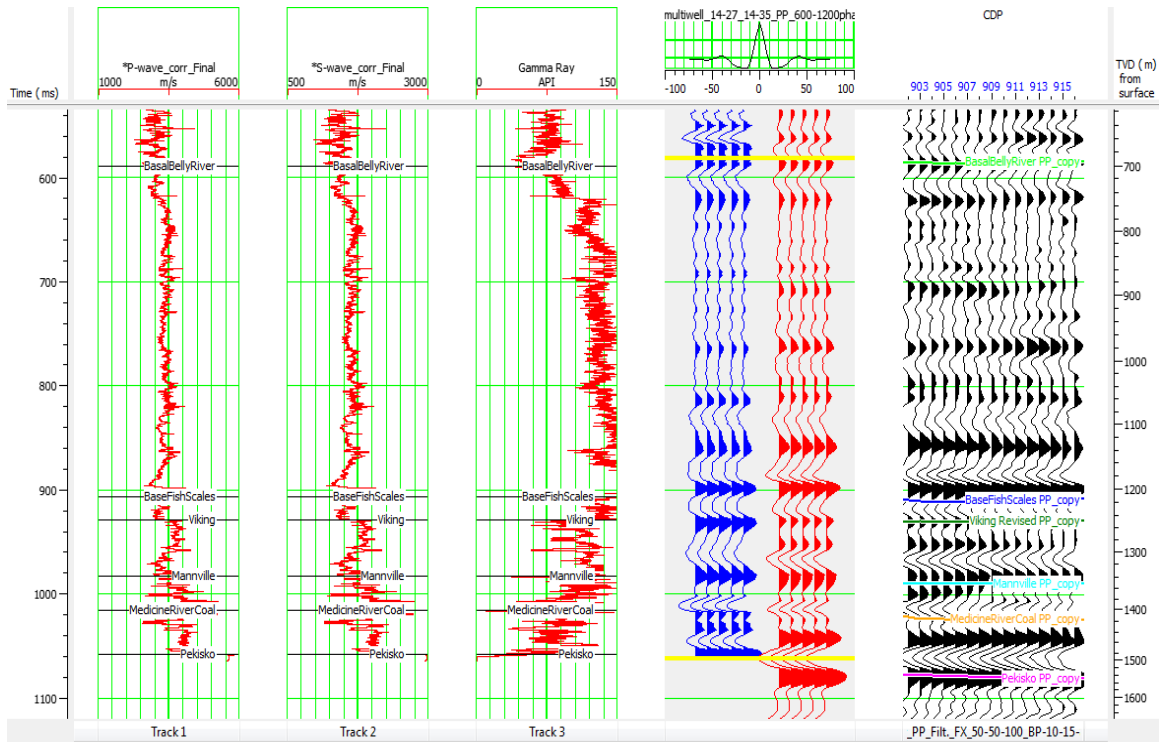


FIG. 10: The final tie of well 14-27 on the PP section; the blue traces represent the synthetic seismogram and the red traces are the extracted trace from the seismic data near the well location.

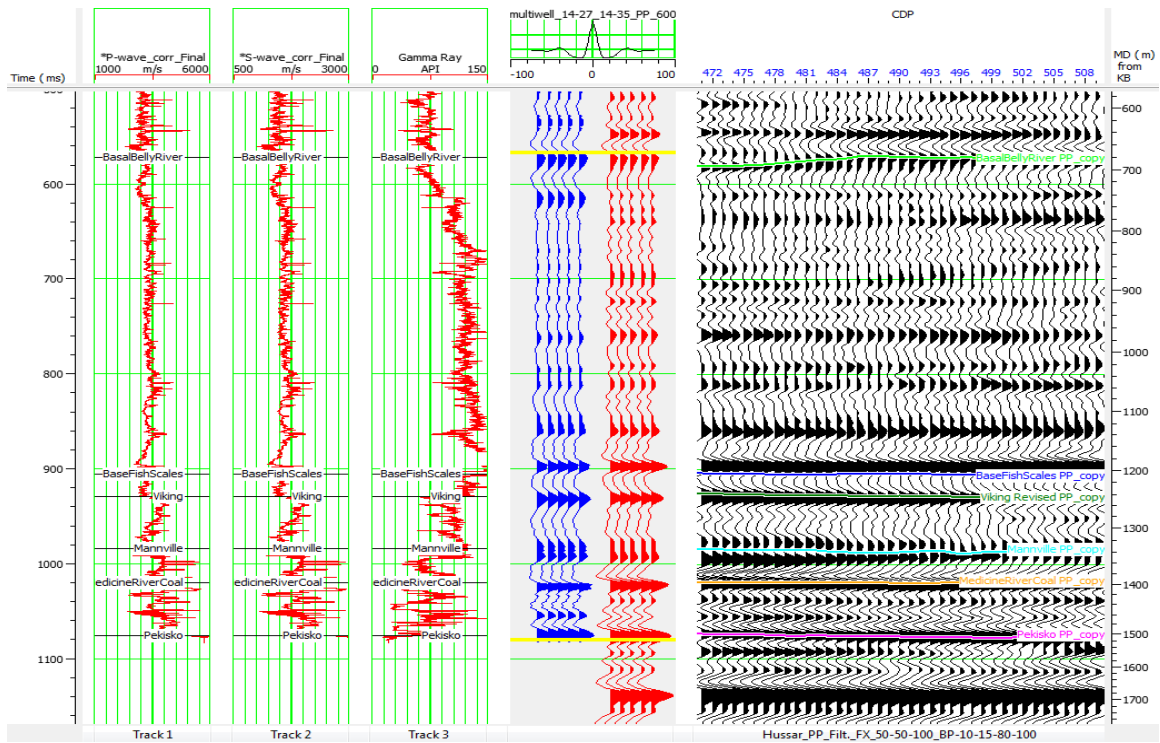


FIG. 11: The final tie of well 14-35 on the PP section; the blue traces represent the synthetic seismogram and the red traces are the extracted trace from the seismic data near the well location.

Synthetics are used to assist in the well log calibration process which links seismic events to the corresponding geological markets (ProMC workshop, 2014). Synthetic traces for PS and PP data were created according to conventional Zoeppritz modeling. Zero offset P wave synthetics are normally used for correlation with seismic data. PS waves are not generated at zero offset; however, small offsets will generate converted wave energy. Figure 12 below shows both seismic sections with their PP and PS wave synthetics.

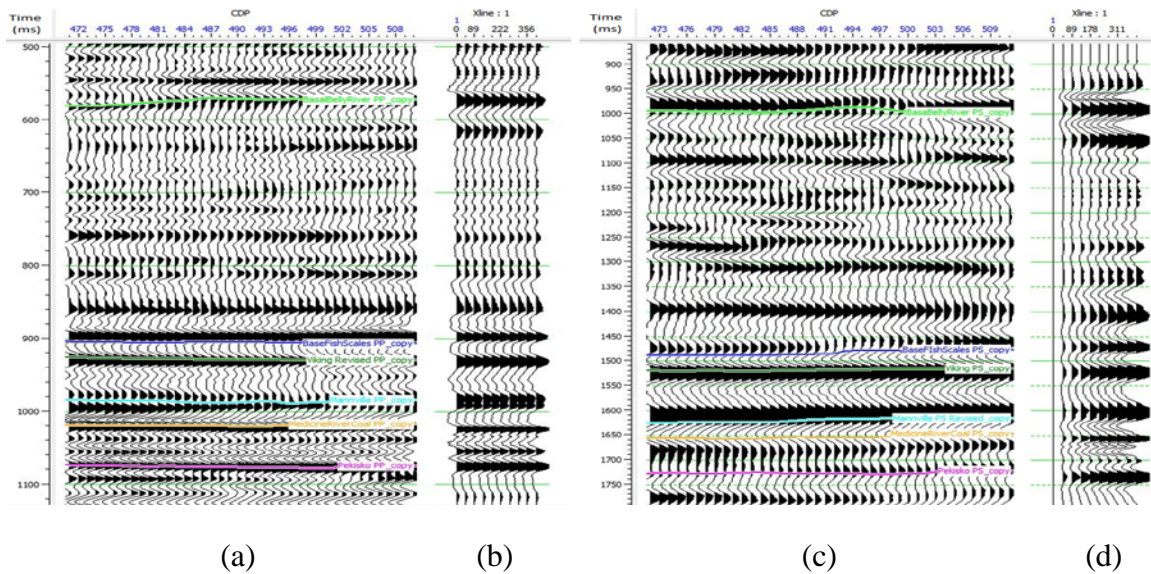


FIG. 12: (a) PP seismic section with horizon picks and (b) PP synthetics offset gather; (c) PS seismic section with horizons picks and (d) PS synthetics offset gather.

### Well Tie Quality Control

Vp/Vs ratio information can be used to verify the consistency of the PP and PS log correlations. This is done by comparing the ratio provided by the corrected P and S sonic logs to the calculated Vp/Vs ratio from the corrected depth-time curves. Both ratio lines were plotted on the same track to check for consistency; when major differences occur they can point to inconsistent correlations in the PP or PS time and would require revision to generate agreement (ProMC workshop, 2014). Agreement is found when Vp/Vs tends to follow the derived values closely. Figure 13 shows the consistency of the ratios at the well.

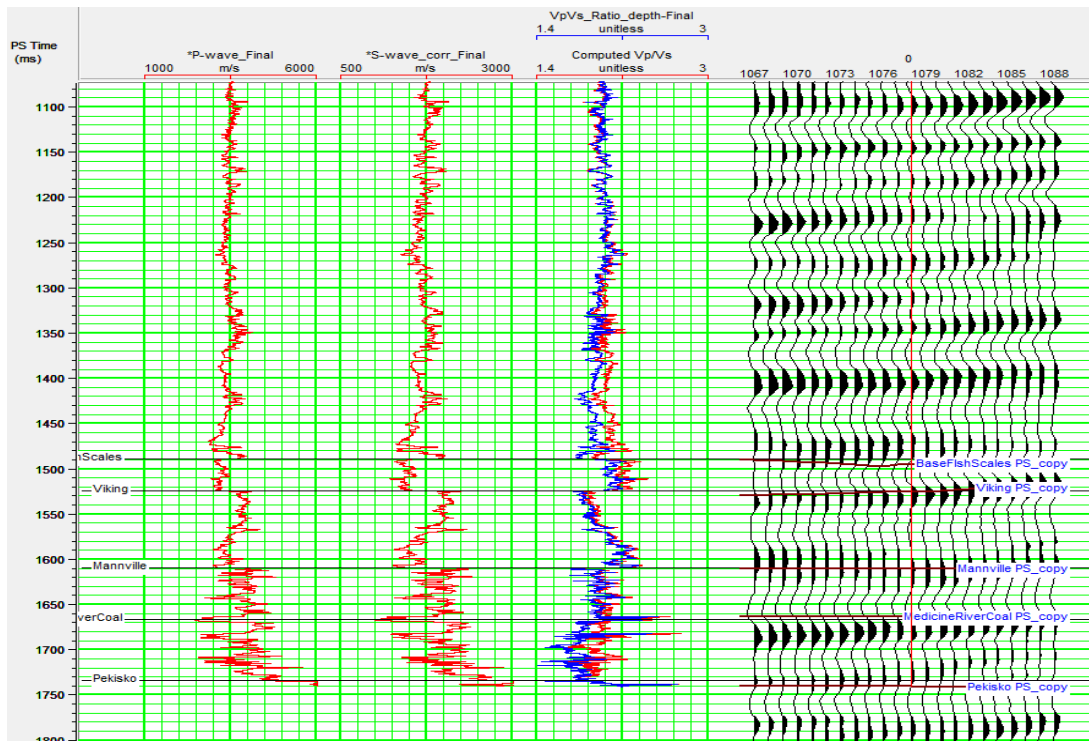


FIG. 13: Quality control on well 12-27; the blue line represents the calculated Vp/Vs ratio from depth-time curves and the red line on the same track represents the ratio derived from the sonic logs; both lines showed consistency in the area of investigation.

## Horizon Picking

Once the events of interest were identified and correlated to both seismic sections, horizons were picked using an automatic picker with manual editing. Intervals of Vp/Vs values between horizons were calculated using the following relationship (Garotta, 1987):

$$Vp/Vs = \frac{(2\Delta Tps - \Delta Tpp)}{\Delta Tpp} \quad (1)$$

In this equation  $\Delta Tpp$  and  $\Delta Tps$  represents the isochrons across the same depth intervals for both PP and PS sections. Horizons were carefully picked and corrected when necessary in order to accurately interpret lateral variations in Vp/Vs. The ratio could be affected due to changes in lithology, porosity, pore fluid, and other formation characteristics (Tatham and McCormack, 1991). A total of six horizons were picked in our analysis; this allowed the study of several isochron intervals for the Vp/Vs error study.

The horizons interpreted on the PP section are shown in Figure 14. In Figure 15b the PS section is plotted at 2/3 the scale of the PP section; both sections are aligned at the same depth intervals and the difference in times is due to the slowness of the S wave which contributes to the PS wave total travel time.

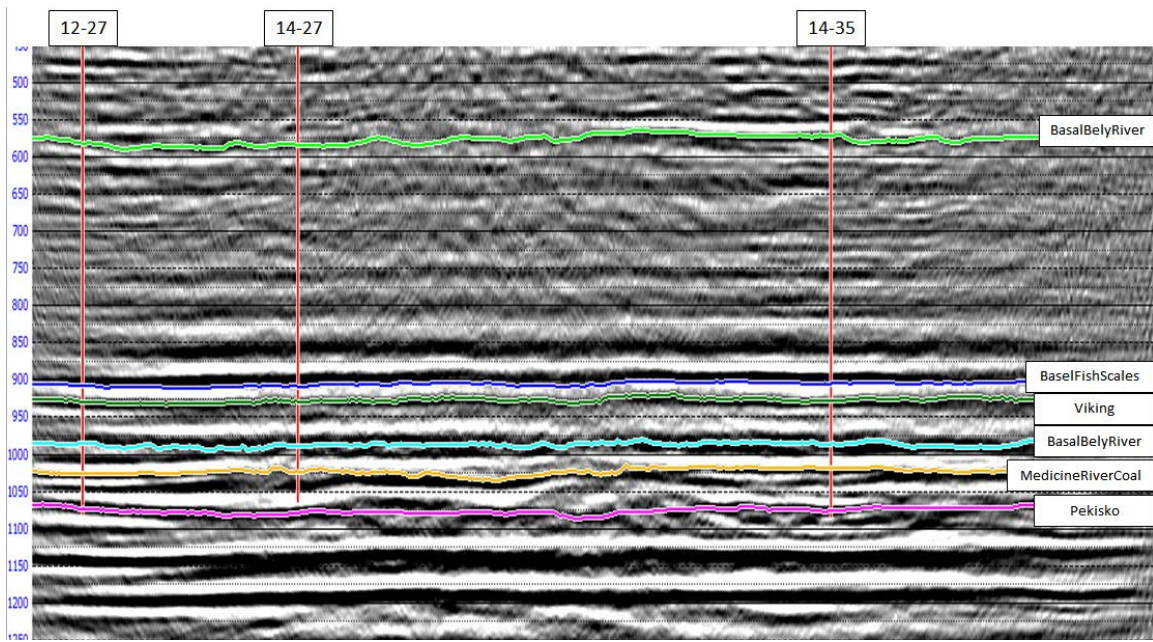


FIG. 14: PP seismic section with six interpreted horizons and the three well locations; well 12-27 provided the dipole sonic logs and the other wells provided only monopole sonic logs.

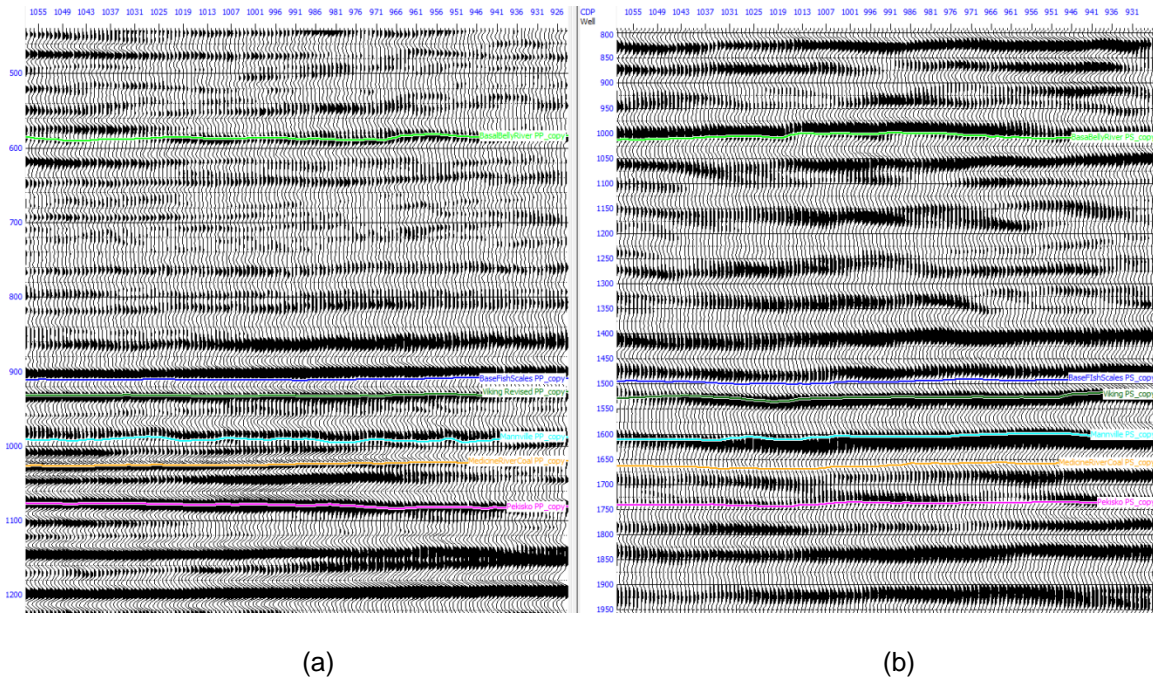


FIG. 15: Interpretation of (a) the PP section and (b) the PS section; the PS section is plotted at 2/3 the scale of the PP section.

In order to improve the interpreted horizon picks, a time shift was applied to each event. When picking horizons, the software would only allow picks to be done at the peak, trough, or zero crossing. After the well ties, the geological tops do not necessarily fall specifically at any of these locations and may differ between PP and PS sections.

Sometimes a time shift is necessary to precisely locate the horizons at the tops and minimize the uncertainty. The first step to find the time shift was to average time differences between the geological top and its interpreted horizons at two well locations (12-27 and 14-35). The average was used to shift the horizon; this step was performed to all the horizons on both PP and PS sections. The improvement to the horizon placement helped reduce the error of  $V_p/V_s$  computed from the isochrons. Figure 16 and 17 show the improvement of the time shift applied to both seismic sections.

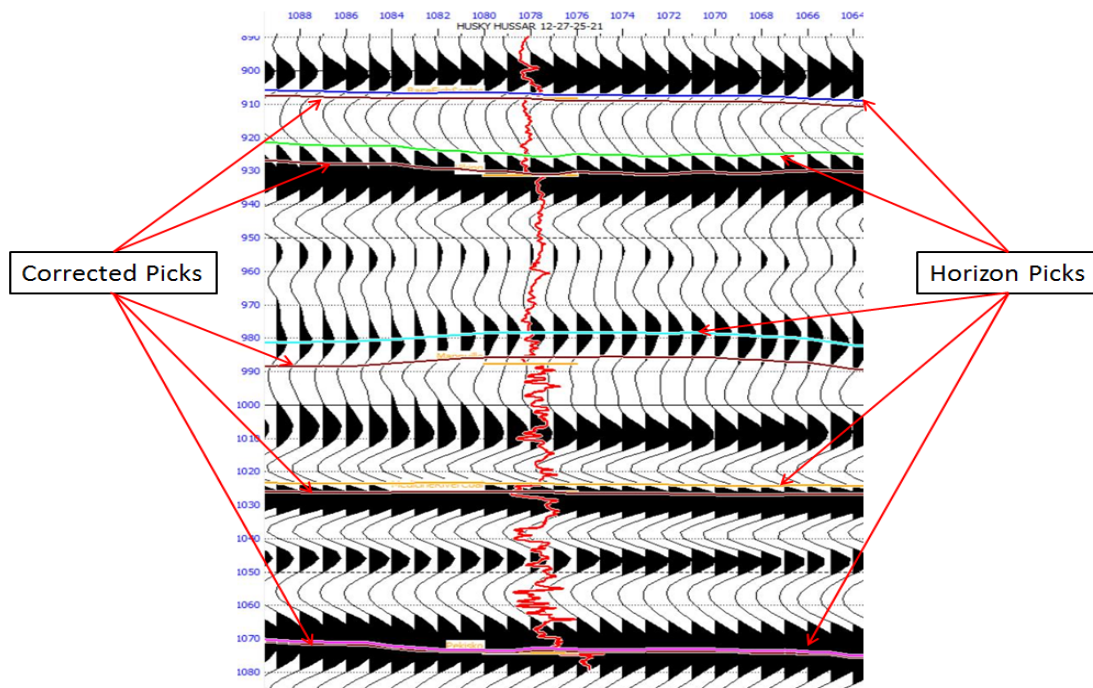


FIG. 16: PP section with interpreted horizons before and after the time shift correction; yellow bars on the logs represent the geological tops.

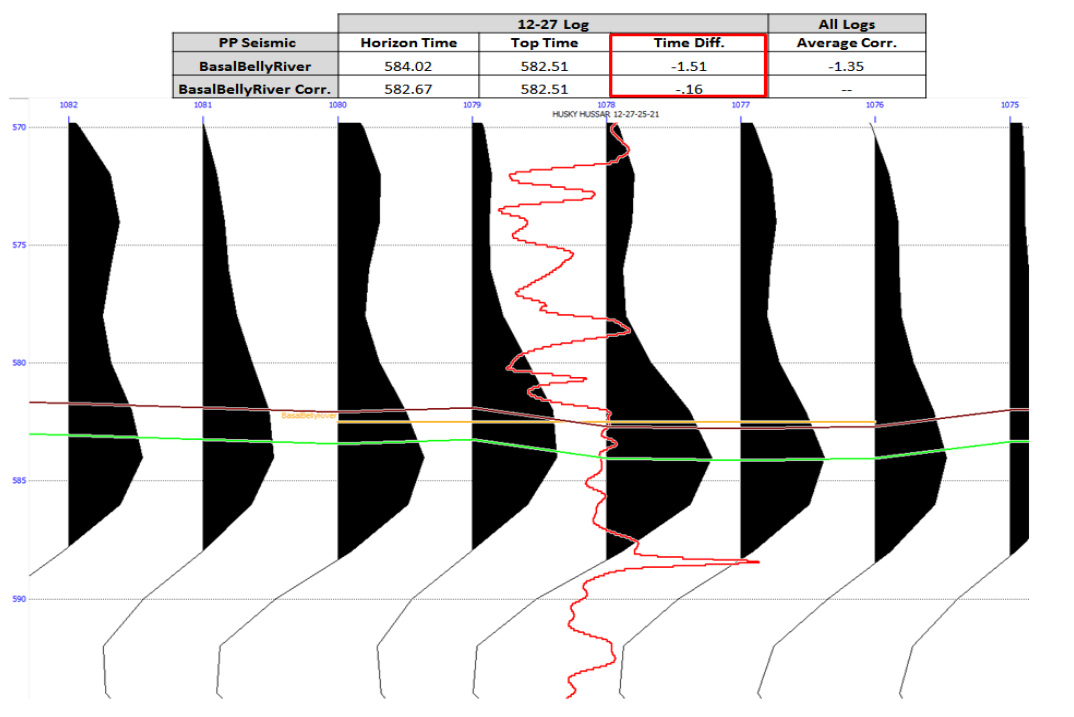


FIG. 17: The table shows the time improvement in the red box after the corrections were applied on the PP section for the BasalBellyRiver horizon. The corrected horizon time is noted in the red box.

## Vp/Vs Error Analysis

To understand the relationship between the sensitivity of Vp/Vs ratios to the time intervals used, we first input the interpreted horizons to create isochrons along the section. A total of eleven isochrons were chosen with intervals ranges from about 22 ms to 500 ms. The table below shows the different intervals in both PP and PS times.

Table 1: Interval times from interpreted horizons.

	PP Time Interval $\Delta T$ (ms)	PS Time Interval $\Delta T$ (ms)
	Average	Average
BasalBellyRiver-BaseFishScales	327.98	487.11
BaseFishScales-Viking	22.55	34.64
Viking-Manville	56.46	79.98
Mannville-MedicineRiverCoal	38.12	56.77
MedicineRiverCoal-Pekisko	47.45	75.43
BasalBellyRiver-Pekisko	496.65	738.02
BasalBellyRiver-MedicineRiverCoal	443.59	658.51
BasalBellyRiver-Mannville	407.05	601.74
BaseFishScales-Pekisko	167.20	245.87
Mannville-Pekisko	89.60	132.21
Viking- Pekisko	146.89	212.19

Vp/Vs calculations for each interval were compared with one another to find patterns and differences (Figures 18 and 19). The results show that the deviations for smaller isochrons were greater than those for larger isochrons. Based on the results, the Vp/Vs ratio calculations are found in part to be dependent on the time interval chosen. Horizon interpretation mis-picks will result in greater error in the calculations for small intervals.

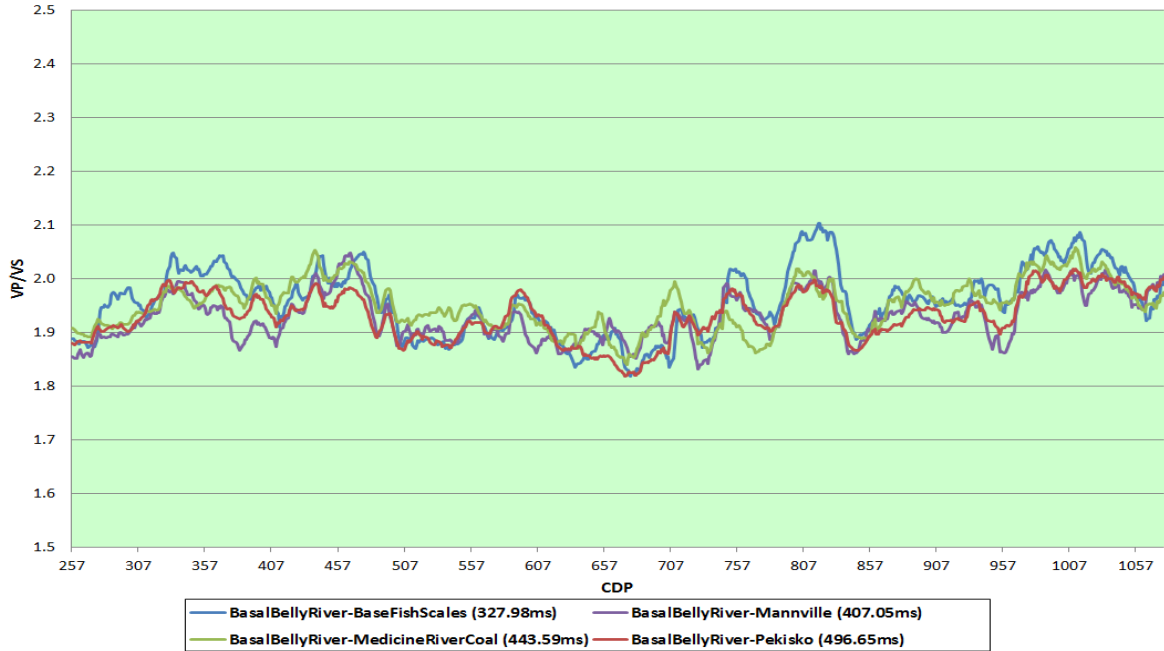


FIG. 18: VpVs curves for large isochrons.

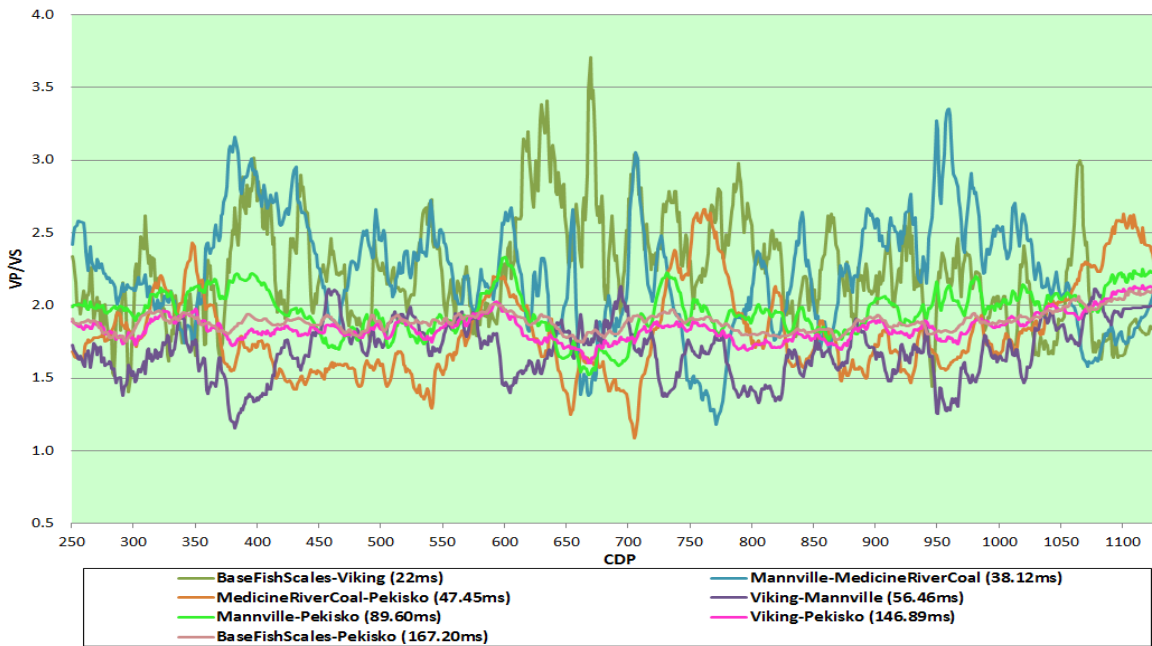


FIG. 19: VpVs curves for small isochrons.

Many factors can influence Vp/Vs ratio values, such as the lithology and pore fluids. A lithology investigation was conducted to understand how this could influence the results. The relationship between Vp and Vs shown in Figure 20 is quasi-linear. The relationship between the gradient and the lithology, especially the shale content, is a subject for further investigation. Crossplots were created from well log curves from well 12-17. Figure 21 shows Vp versus Vs crossplot; the color key shows gamma ray (GR) log where the lower values (GR<50 API) corresponds to cleaner sandstones. These crossplots are from the area of investigation which covers the Mannville formation.

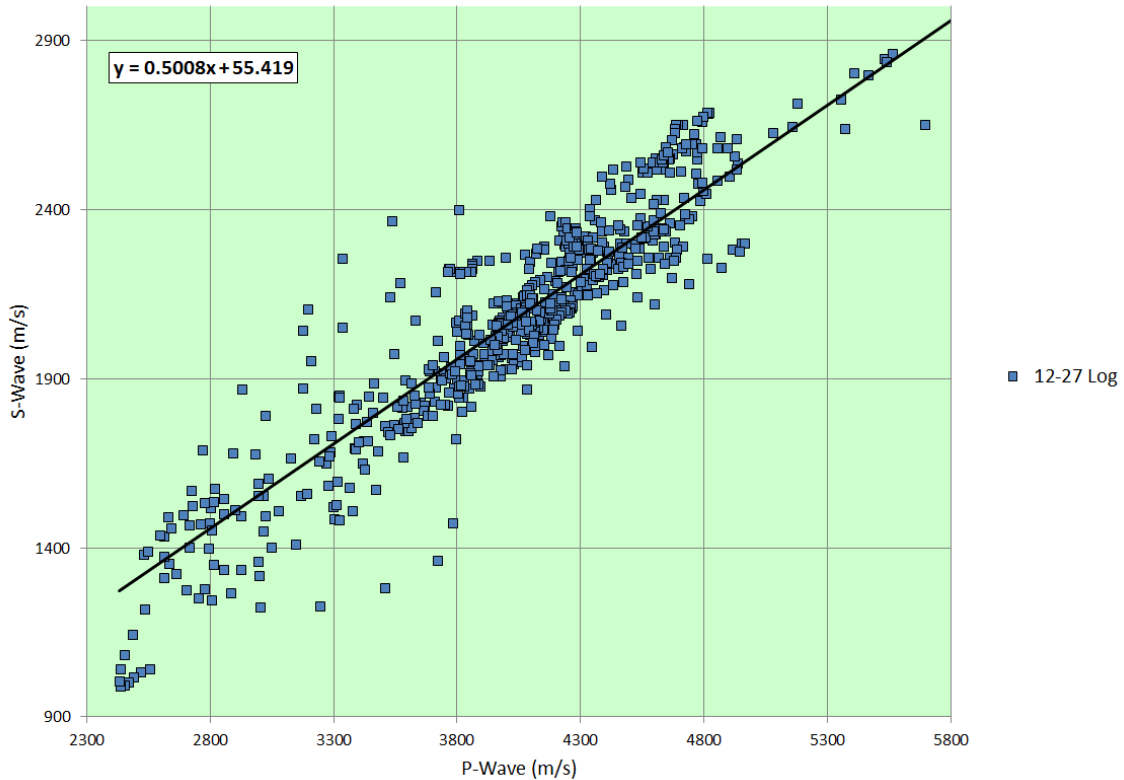


FIG. 20: Vp against Vs crossplot with gradient line of 0.50 for well 12-27.

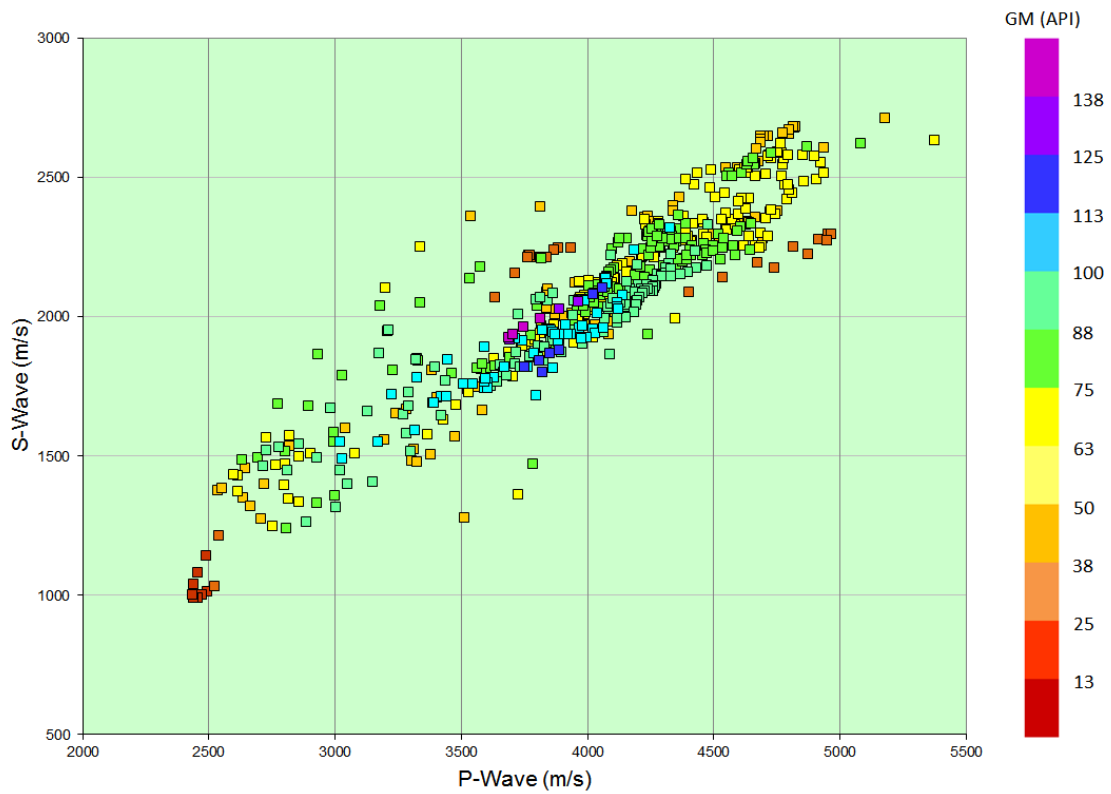


FIG. 21: Crossplot  $V_p$  against  $V_s$  (Color: Gamma-Ray) in well 12-27.

The plot of  $V_p$  against  $V_p/V_s$ , as shown in Figure 22, shows a lot of scatter that the  $V_p/V_s$  ratio increases as  $V_p$  increases. The basis of much of the lithology work in PS exploration relates to anomalous changes in  $V_s$  with respect to  $V_p$  (Stewart et al., 2002). A changing  $V_p/V_s$  value is often closely tied to a changing lithology (Rider, 1996) and perhaps pore geometry.  $V_p/V_s$  values cluster between 1.9 and 2.0 at relative high P wave and rest of the samples are very scatter.

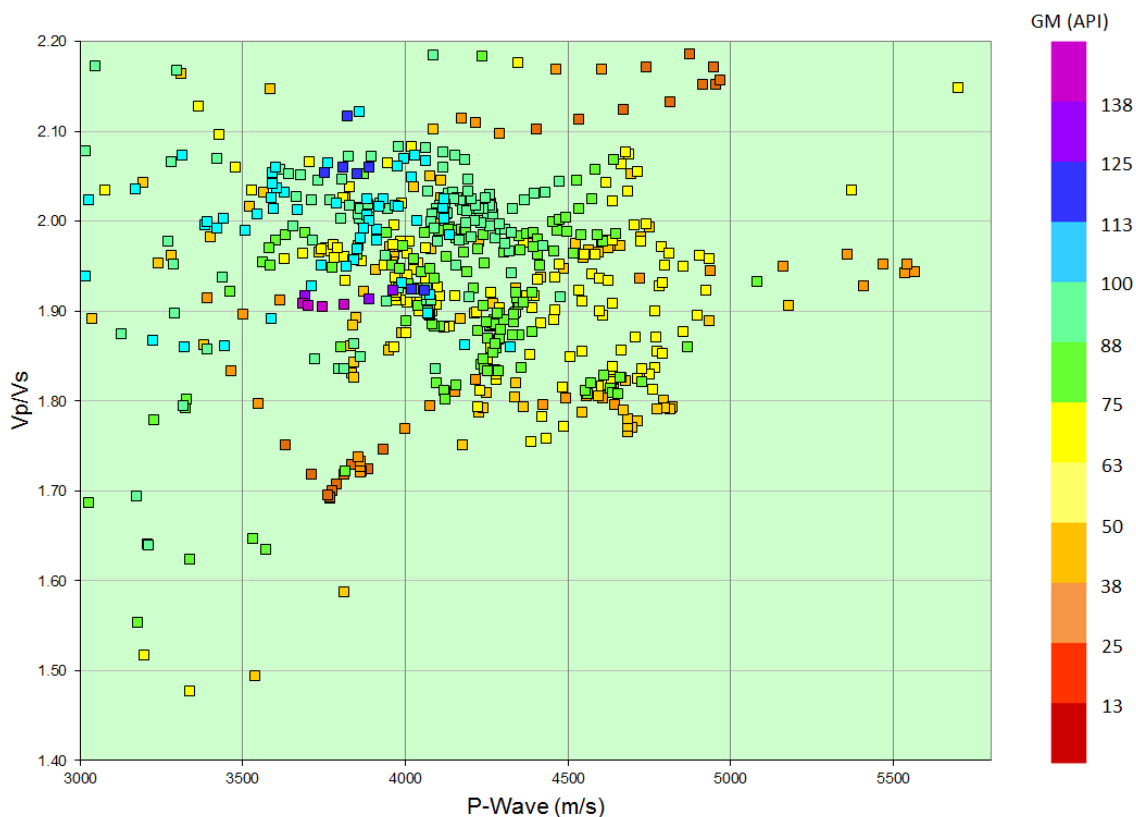


FIG. 22: Crossplot Vp versus Vp/Vs values for well 12-27.

The plot of the Vp/Vs ratio against gamma log values for well 12-27 is shown in Figure 23. The data points are very scattered, although there is a general trend of Vp/Vs increasing with increasing gamma log values, which in turn could reflect an increase in shale content. The majority of the data points from well 12-27 have API values less than 100 and there is a dense cluster of points with values of 60 to 95 API. Most points from well 12-27 at the glauconitic formation have Vp/Vs values ranging from 1.76 to 1.95; these values are indicative of sandstone lithologies.

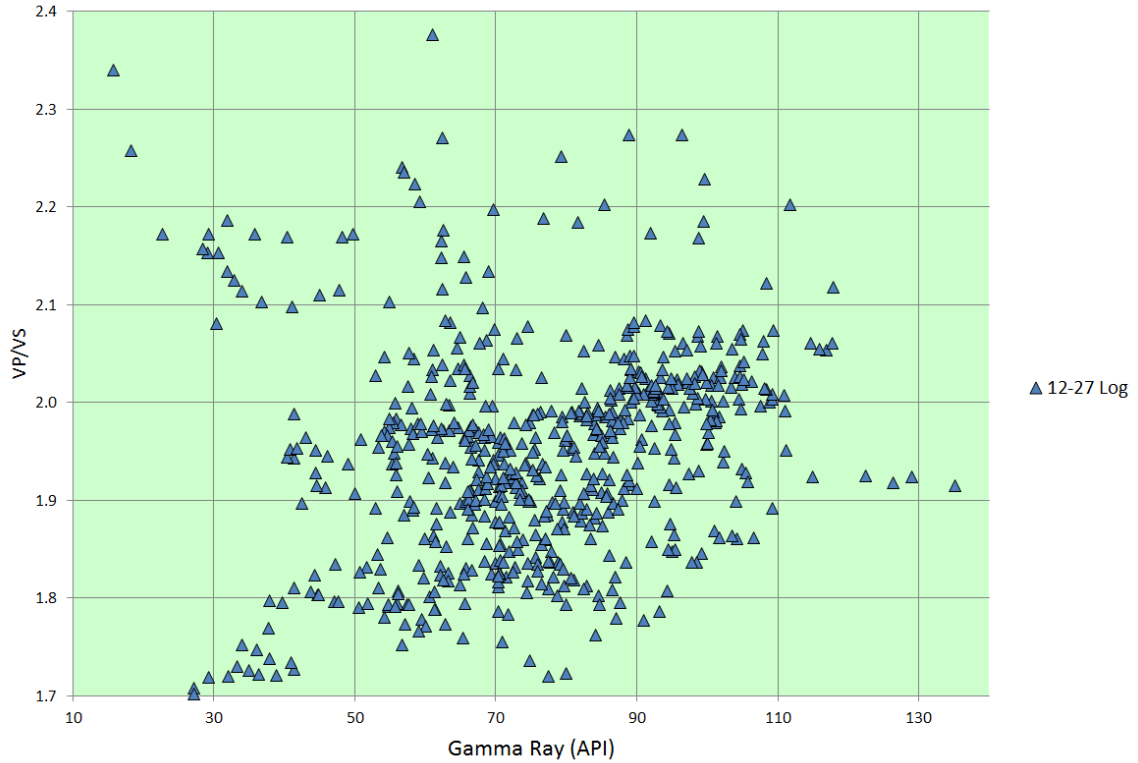


FIG. 23: Crossplot of gamma-ray against Vp/Vs values for well 12-27.

### Error Analysis on Vp/Vs

To estimate the error for the Vp/Vs analysis, propagation of error method was used. This method calculates the error in the values of a function based on the effects of the uncertainty of the variables on the function (Louro, 2014). An uncertainty of  $\pm 2$  ms was used for the horizon picks in order to find the uncertainty in Vp/Vs. In this case, the function used to calculate Vp/Vs (equation 1) has two variables:  $\Delta T_{pp}$  and  $\Delta T_{ps}$ . According to the propagation of error equation, if a function  $y$  depends on the variables  $x_1, x_2, \dots, x_n$ , where  $x_i$  is measured with uncertainties  $u(x_i)$ , the uncertainty in the calculated value  $y$  is given by

$$u(y) = \sqrt{c_1^2 u(x_1)^2 + c_2^2 u(x_2)^2 + \dots + c_n^2 u(x_n)^2} \quad (2)$$

where  $c_i$  are called sensitivity coefficients because they provide information about how sensitive  $y$  is to uncertainties in each of the variables. Each sensitivity coefficient is the partial derivatives of  $y$  with respect to each  $x_i$ :

$$c_i = \frac{\partial y}{\partial x_i}$$

To simplify the expression, the variables  $\Delta T_{pp}$  and  $\Delta T_{ps}$  were substituted by  $z$  and  $x$ , respectively and  $V_p/V_s$  was substituted by the variable  $y$ . The sensitivity coefficients can then be written as

$$c_1 = \frac{\partial y}{\partial x} = \frac{\partial}{\partial x} \left( \frac{2x - z}{z} \right) = \frac{2}{z};$$

$$c_1^2 = \frac{4}{z^2} \quad (3)$$

$$c_2 = \frac{\partial y}{\partial z} = \frac{\partial}{\partial z} \frac{(2x - z)}{z} = \frac{2\sqrt{x}}{z^2};$$

$$c_2^2 = \frac{4x}{z^4} \quad (4)$$

Then substituting equations 3 and 4 into 2, and with the uncertainties  $u(x)$  and  $u(z)$  equal to  $\pm 2$  ms, the final absolute error equation for  $V_p/V_s$  will be given by

$$v_{p/vs} (error) = \sqrt{\frac{4}{z^2} u(x)^2 + \frac{4x^2}{z^4} u(z)^2};$$

$$v_{p/vs} (error) = 4 \sqrt{\frac{1}{\Delta T_{pp}^2} + \frac{\Delta T_{ps}^2}{\Delta T_{pp}^4}} \quad (5)$$

Relationships between the time interval,  $\Delta T$ , and both the standard deviations and error in  $V_p/V_s$  were studied. The standard deviation was calculated from the computed ratio analysis for each interval. It was noted that the deviation tends to decrease as the interval length  $\Delta T$  becomes larger (Figure 24). The best fit line in red shows that the deviation is nearly constant at large time intervals, but exponentially increases as the interval approaches 150 ms. The line increases asymptotically as it approaches zero milliseconds.

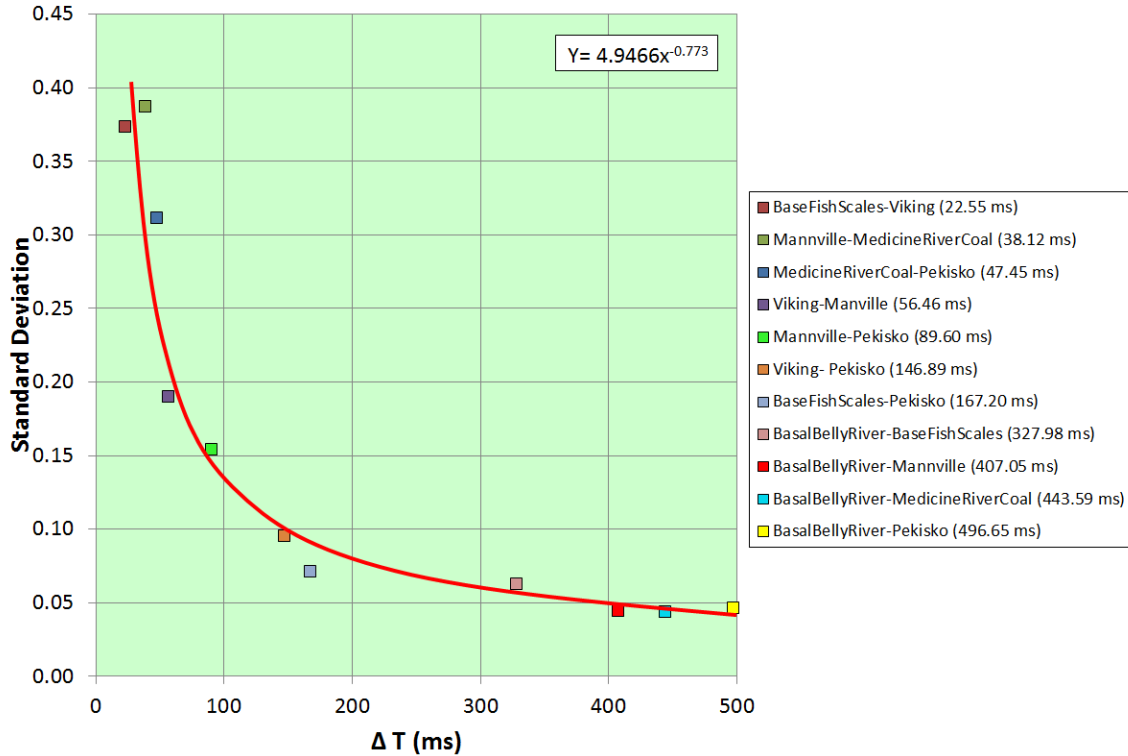


FIG. 24: Crossplot of standard deviation in Vp/Vs analysis against the time interval; the best fit line in red exponentially increases at intervals less than 150 ms.

The uncertainty in the Vp/Vs ratio was used to understand how  $\Delta T$  can affect the percent relative error in the ratio analysis (Figure 25). Time intervals above 150ms corresponded to percent error values that were consistently low, ranging from 0.74 to 2.20 percent. For intervals below this threshold, the percent error increased exponentially; the smallest time intervals in our study were approximately 22 and 38 milliseconds and their corresponding percent error were 16.52 and 9.76 percent respectively. The calculation for the error assumes an uncertainty of  $\pm 2$  ms in the interpretation from the horizons picks.

A crossplot using average Vp/Vs values with error bars versus  $\Delta T$  (Figure 26) show how the uncertainty affects the analysis. Error bars represent the variability of data, in this case Vp/Vs, and it is used here to indicate the error. The line in red is the average of all the Vp/Vs values, and the dashed line indicates values one standard deviation away from this mean. All the points with a  $\Delta T$  larger than 150 ms fall within one standard deviation of the average of the Vp/Vs ratio and are associated with an uncertainty that does not significantly affect Vp/Vs. The majority of the points with  $\Delta T$  less than 150 ms fall outside of the one standard deviation, which could be due to either uncertainty or the lithology of the geological area. The uncertainty in the values with a small time interval is large enough to significantly affect the Vp/Vs analysis.

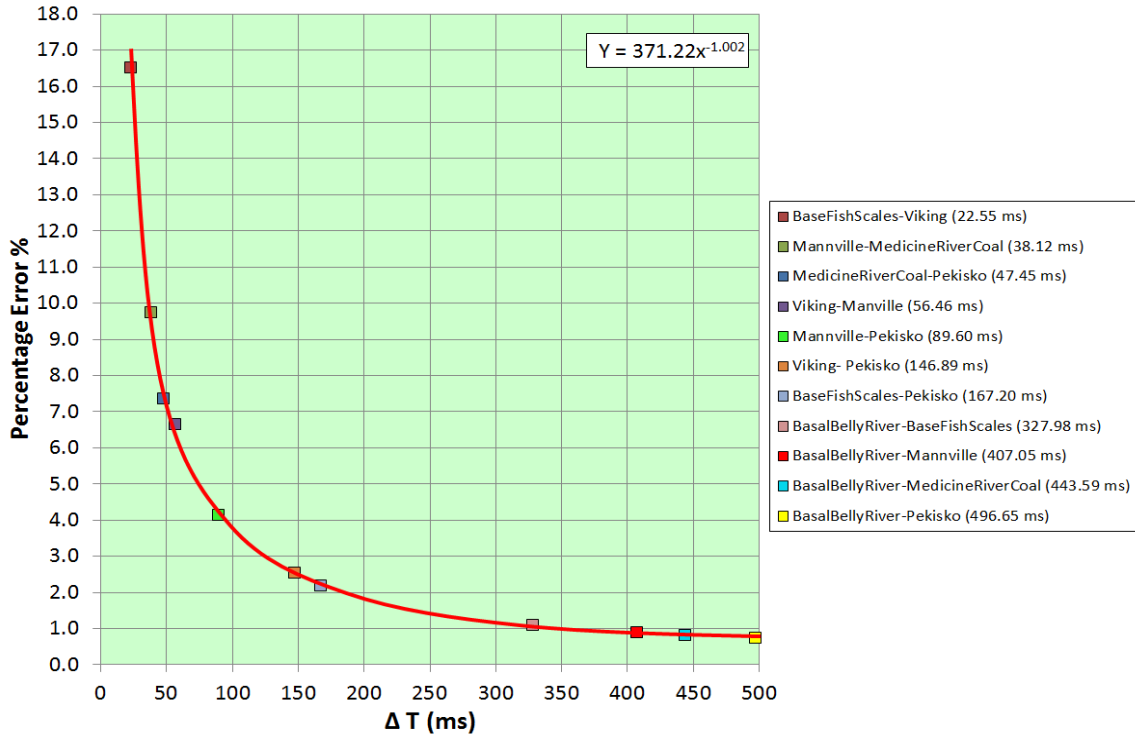


FIG. 25: Crossplot of percent relative error in Vp/Vs versus ΔT; the error tends to increase as the time interval becomes smaller.

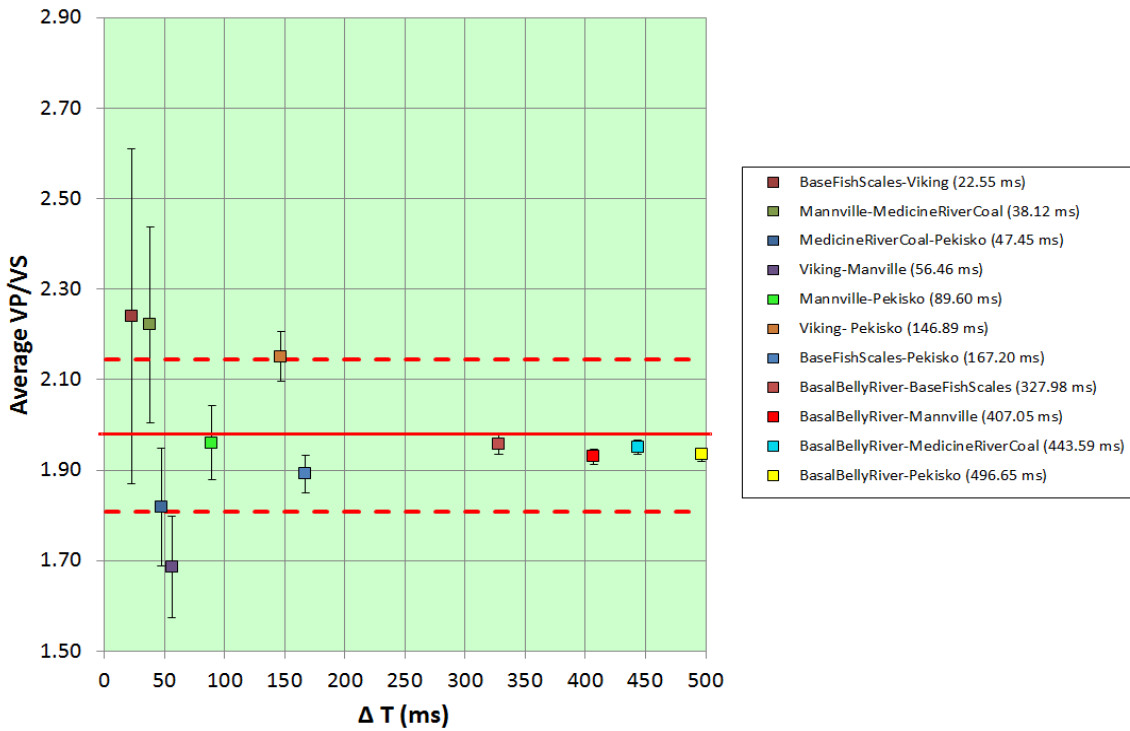


FIG. 26: Crossplot of average Vp/Vs versus ΔT; error bars represent the amount of uncertainty; the solid red line represents the average Vp/Vs value and the dashed red lines represent values one standard deviation away from the mean.

## SYNTHETIC MODEL

A synthetic model was created to compare the error results from the real data to results from this model. The model analysis provided ideal conditions in which well synthetic seismograms would achieve a high correlation to the synthetic seismic model and reduce uncertainty in the analysis. The first step for this analysis was to create a layered model; this model had horizontal interfaces with various thickness for each layer (Figure 27). The next step was to create the synthetic P and S sonic logs that would match the model. A density log was also created using a Gardner relationship.

The wells were correlated to the PP and PS volumes and lateral Vp/Vs ratios were calculated. The model assumed an isotropic medium for each layer. Well synthetic seismograms were created (Figures 28 and 29) to tie the wells to the synthetic seismic volume (Figure 30). Ricker wavelets (Figure 31) were used to create synthetic seismograms. The dominant frequencies were 40 Hz and 25Hz for PP and PS respectively.

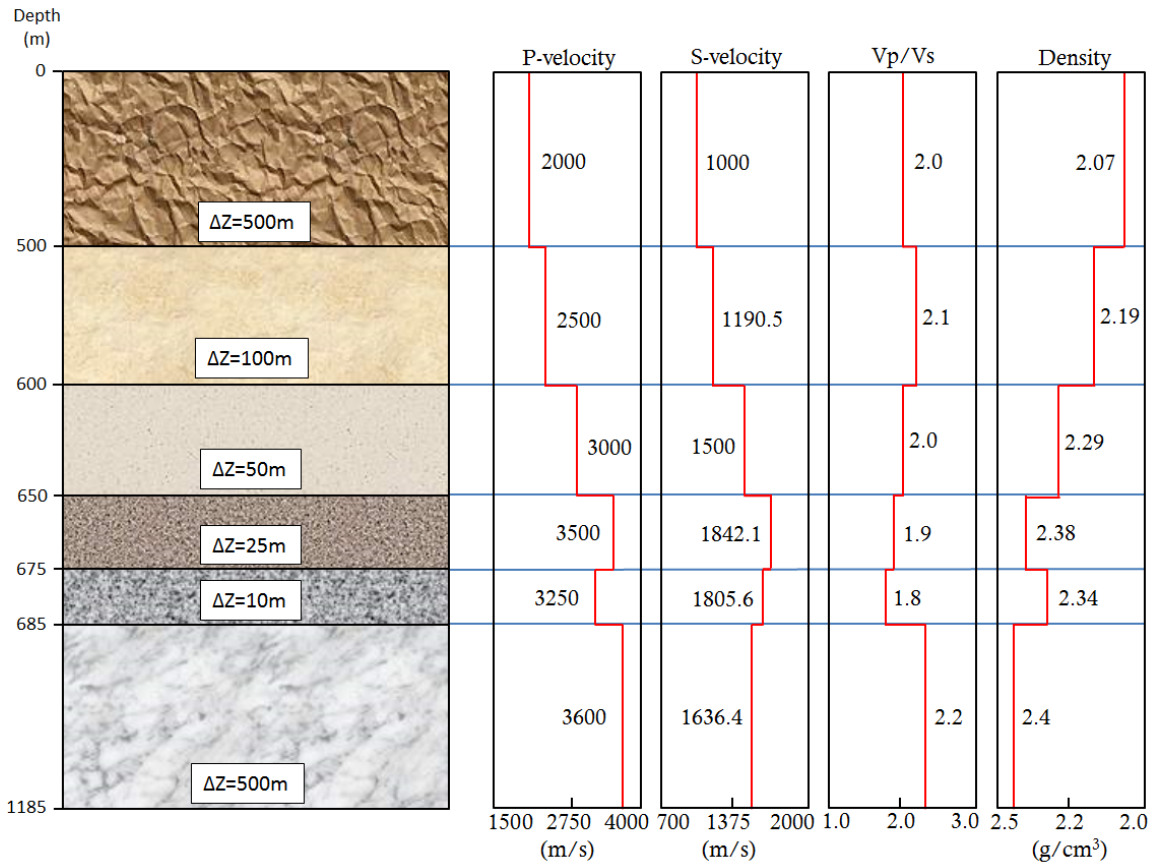


FIG. 27: Layered model and synthetic logs.

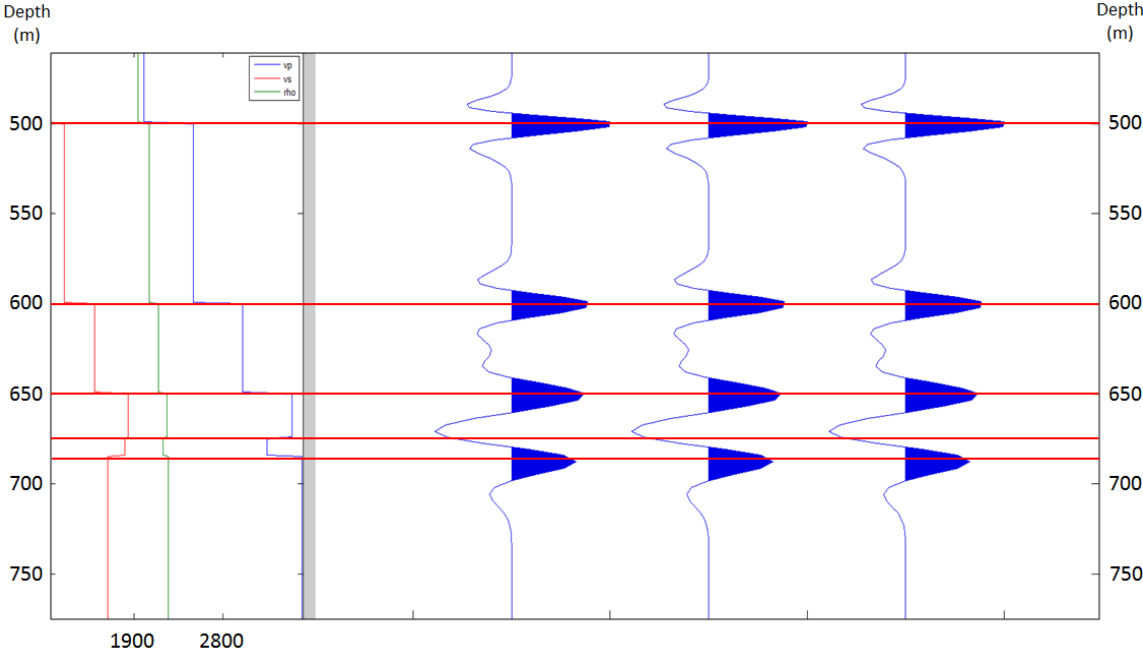


FIG. 28: Well synthetic seismogram for PP wave.

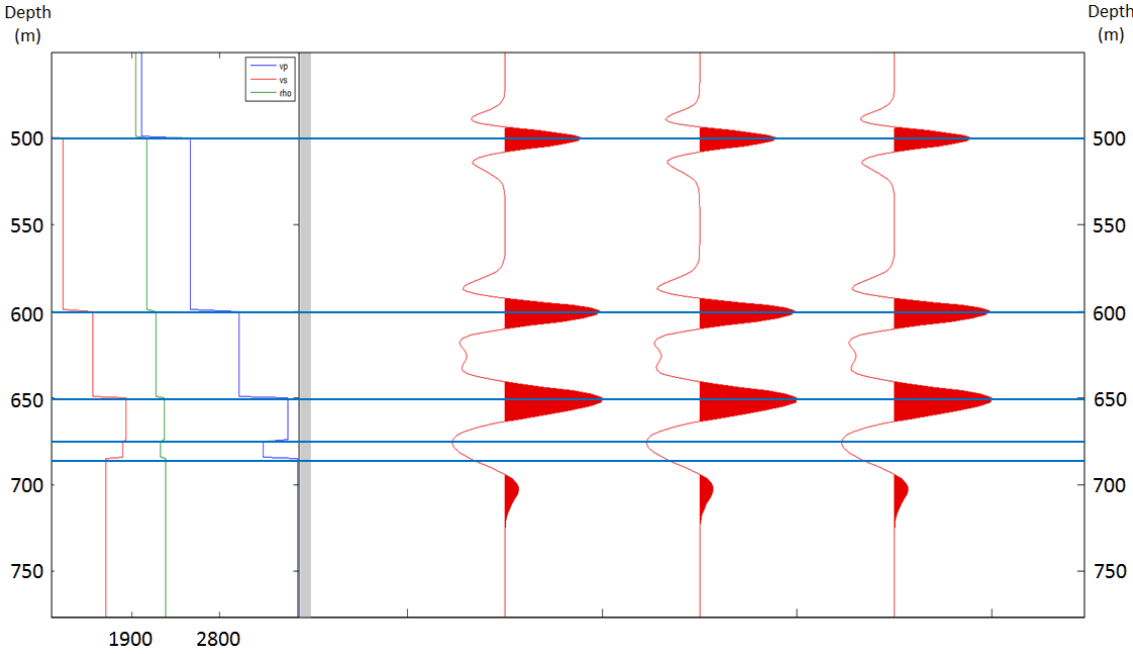


FIG. 29: Well synthetic seismogram for PS wave.

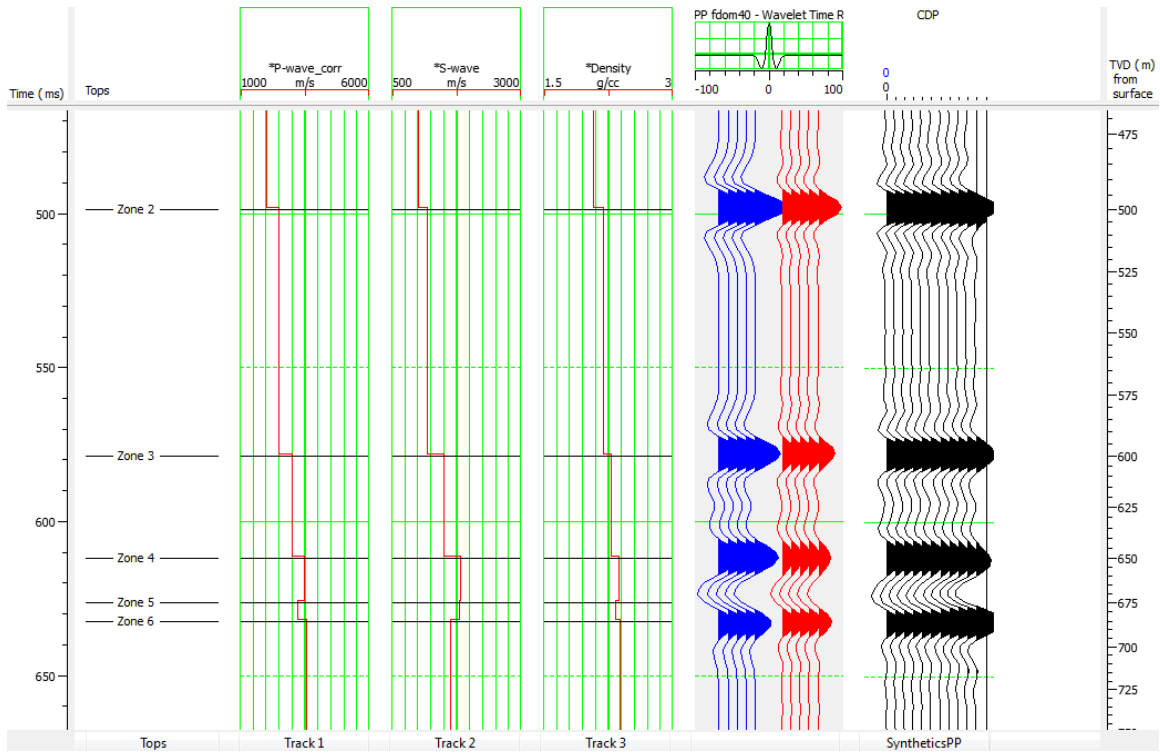
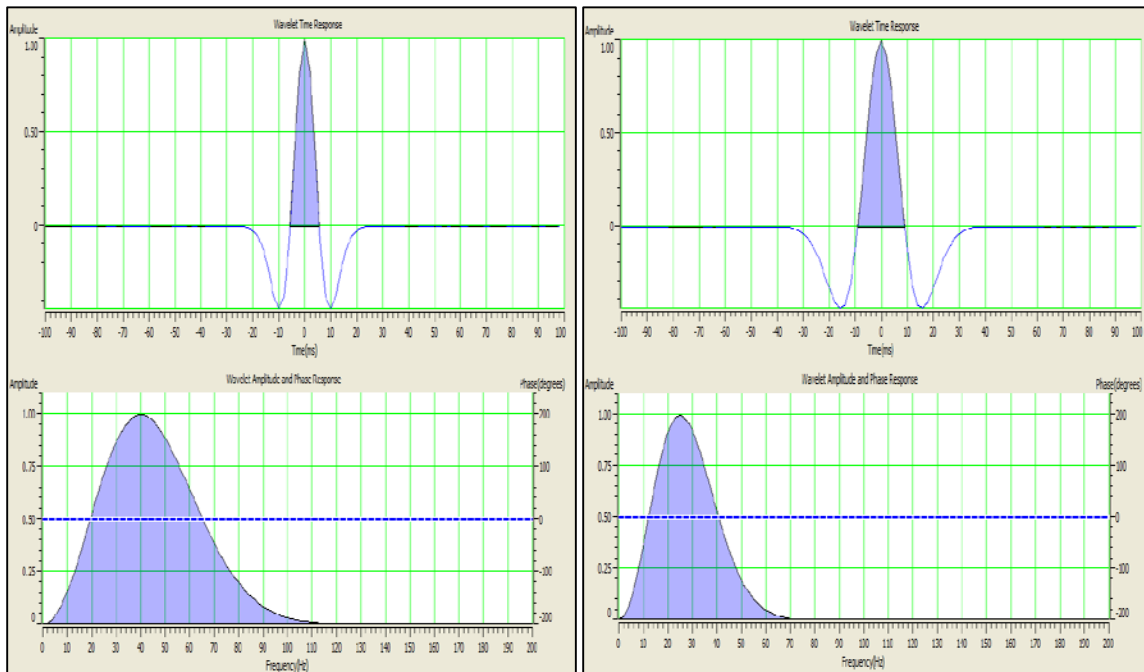


FIG. 30: PP well tie for synthetic model.



(a)

(b)

FIG. 31: (a) PP synthetic wavelet with dominant frequency of 40Hz and (b) PS synthetic wavelet with dominant frequency of 25Hz.

Due to the model being completely isotropic and having completely horizontal interfaces, the deviation analysis was zero for each layer. This means that at any offset point of the layer, the value for Vp/Vs remained constant. Calculations for Vp/Vs (Figure 32) were done using the Garotta equation and an error analysis was performed for each interval.

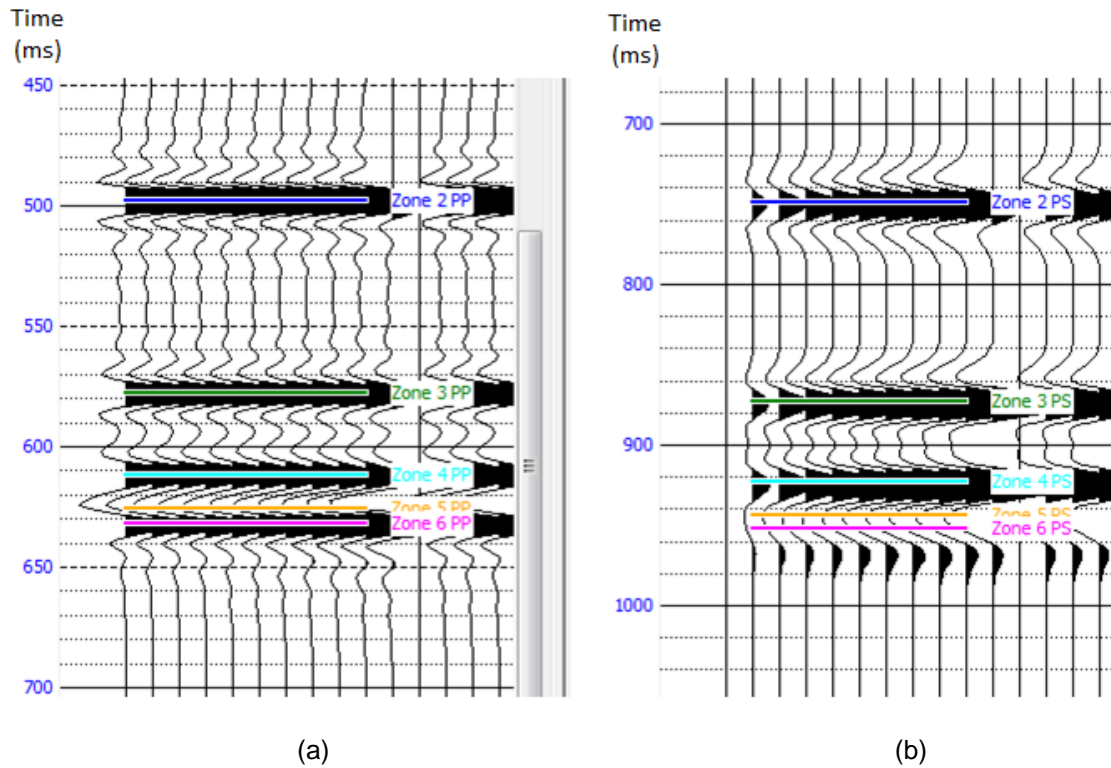


FIG. 32: Interpretation of (a) the PP model section and (b) the PS model section; the PS section is plotted at 2/3 the scale of the PP section.

The correlation between seismic and well synthetics was a perfect match. Thus, there is no uncertainty in the horizon interpretation and consequently no error is present. Figure 33 shows a plot of the average Vp/Vs values from the synthetic model versus  $\Delta T$ . The horizon picks exactly matched the geological tops depths at the well. The results were Vp/Vs values with no variability associated with them.

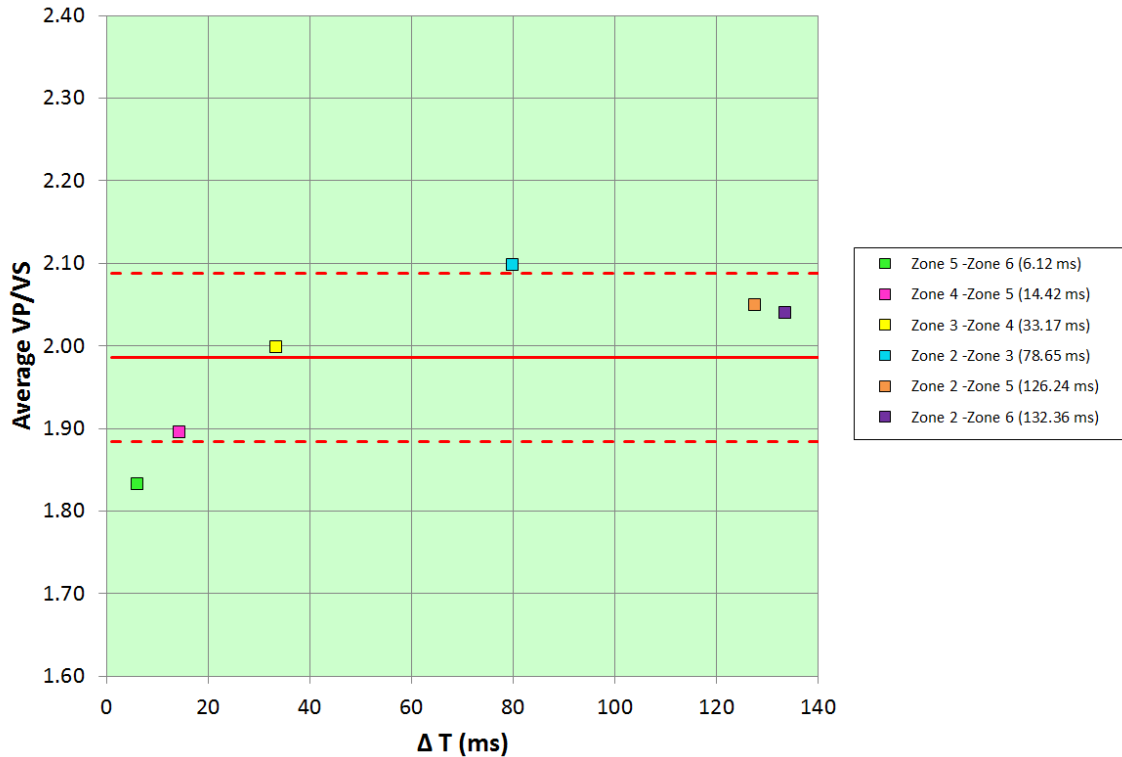


FIG. 33: Crossplot of the average Vp/Vs ratio versus  $\Delta T$

## CONCLUSION

Analysis performed on the Hussar data indicates that the uncertainty in Vp/Vs values will increase as time interval becomes smaller. It is important for interpreters to understand this relationship in order to avoid erroneous results in interval Vp/Vs analysis. Based on the increasing behavior of error with respect to decrease in the time interval, as well as taking into consideration the variability of the Vp/Vs values due to uncertainty it is suggested to use isochron intervals greater than 150 ms. Interval Vp/Vs analysis for data with intervals greater than this time presented low uncertainty

## ACKNOWLEDGEMENT

The author would like to thank my supervisor and CREWES sponsors, especially CGG Veritas for providing the interpretation software Hampson-Russell and Gedco for providing Vista and CREWES for providing Syngam. We also gratefully acknowledge support from NSERC (Natural Science and Engineering Research Council of Canada). Also, the author extends appreciation to the entire CREWES staff, especially Helen Isaac, and to all the students in CREWES.

## REFERENCES

- Allan, J. A. and Rutherford, R. L., 1934, *Geology of Central Alberta*: Alberta Geological Survey, Report 30. Retrieved July 22nd, 2013: [http://www.ags.gov.ab.ca/publications/abstracts/REP\\_30.html](http://www.ags.gov.ab.ca/publications/abstracts/REP_30.html).
- Garotta, R., 1987, Two-component acquisition as a routine procedure, in Danbom, S.H., and Domenico, S.N., Eds., *Shear-wave exploration*: Soc. Expl. Geophys., Geophysical development series 1, 122-136.
- Gavotti, P., Lawton D., 2014, Post-stack inversion of the Hussar low frequency seismic data: Crewes thesis document.
- Isaac, J. H. and Margrave, G. F., 2011, Hurrah for Hussar! Comparisons of stacked data: CREWES Research Report, 23, No. 55.
- Louro, A. A., 2014, Measurement uncertainties. Physics 255 [lecture notes]. Retrieved from <http://www.pjl.ucalgary.ca/courses/physics255/labs/Measurement-Uncertainties-WI2014.pdf>
- Margrave, G. F., Mewhort, L., Phillips, T., Hall, M., Bertram, M. B., Lawton, D. C., Innanen, K. A. H., Hall, K. W. and Bertram, K. L., 2011, The Hussar low frequency experiment: CSEG Recorder, 37, No. 07, 25-39.
- Miller, S. L. M., 1996, Multicomponent seismic data interpretation: M.Sc. thesis, Univ. of Calgary.
- Mossop, G. D., Shetsen, I (comp.), 1994, *Geological Atlas of the Western Canada Sedimentary Basin*. Retrieved August 14th, 2013: [http://www.ags.gov.ab.ca/publications/wcsb\\_atlas/atlas.html](http://www.ags.gov.ab.ca/publications/wcsb_atlas/atlas.html).
- ProMC workshop, 2014, *Hampson-Russell Software Documentation*. Hampson-Russell Software, a CGGVERTIAS Company.
- Rider, M., 1996, *The geological interpretation of well logs*, 2nd ed.: Whittles Publishing.
- Simm, R., Bacon, M., 2014, *Seismic Amplitude: An interpreter's handbook*. Cambridge University Press.
- Smith, D.G., 1994, Paleogeographic evolution of the Western Canada Foreland Basin. In: *Geological Atlas of the Western Canada Sedimentary Basin*. G.D. Mossop and I. Shetsen (comps.). Calgary, Canadian Society of Petroleum Geologists and Alberta Research Council, chapter 17.
- Stewart, R. R., Gaiser, J. E., Brown, R. J., and Lawton, D. C., 2002, Converted-wave seismic exploration: *Methods: Geophysics*, **67**, 7, 1–16.
- Sheriff, R.E., Geldart, L. P., 1995, *Exploration Seismology* (2nd ed.). Cambridge University Press.
- Tatham, R.H. and McCormack, M.D., 1991, Multicomponent seismology in petroleum exploration, investigation in *Geophysics Series* vol. 6, SEG.
- Widess, M.B., 1973, How thin is a thin bed?: *Geophysics*, **38**, 1176-1180.